

International Journal of Heat and Mass Transfer

A NEW POOL BOILING HEAT TRANSFER MODEL FOR WETTING DIELECTRIC FLUIDS ON METAL FOAMS

--Manuscript Draft--

Manuscript Number:	HMT-D-20-03041
Article Type:	Full Length Article
Keywords:	pool boiling; metal foam; dielectric fluid; predictive model; immersion cooling
Corresponding Author:	Elaine Maria Cardoso UNESP - Universidade Estadual Paulista Ilha Solteira, Sao Paulo Brazil
First Author:	Leonardo Lachi Manetti
Order of Authors:	Leonardo Lachi Manetti
	Ana Sofia Oliveira Henriques Moita
	Elaine Maria Cardoso
Abstract:	<p>Porous structures, as metal foams, can enhance the heat transfer performance. For a safe industrial application, a predictive model for both heat transfer coefficient and maximum heat flux is required. However, there is no correlation for dielectric fluids on metal foams available in the literature. This work aims to develop a semi-empirical model based on dimensional analysis for metal foam surfaces in pool boiling with different dielectric fluids. The model takes into account the porous heating surface characteristics (porosity, pore diameter, and thickness), the working fluid thermophysical properties, and its interaction. The model was developed based on the experimental database obtained by the authors and validated with the open literature database. Two metal foams with different characteristics were used for carrying out the pool boiling tests with two different working fluids: HFE-7100 and ethanol. The newly developed correlation predicted well the database with an average error equal to 10.8% where 93.8% within the error range of $\pm 30\%$. To the maximum heat flux, the average error was 13.6% where 100% within the error range of $\pm 30\%$. The pore diameter and thickness play an important role in both models. The porosity and solid-phase thermal conductivity from the metal foam change the porous medium thermal conductivity, which influences the heat transfer coefficient (HTC). Finally, the properties of the working fluid also influence the predictive model, mainly the latent heat of vaporization, liquid thermal conductivity, and saturation temperature.</p>
Suggested Reviewers:	
Opposed Reviewers:	

A NEW POOL BOILING HEAT TRANSFER MODEL FOR WETTING DIELECTRIC FLUIDS ON METAL FOAMS

Leonardo Lachi Manetti¹, Ana Sofia Oliveira Henriques Moita^{2,3} and Elaine Maria Cardoso^{1,4}

¹*UNESP – São Paulo State University, School of Engineering, Post-Graduation Program in Mechanical Engineering, Av. Brasil, 56, 15385-000, Ilha Solteira, SP, Brazil*

²*IN+, Dep. Mechanical Engineering, Instituto Superior Técnico, Universidade de Lisboa, Lisbon, Portugal*

³*CINAMIL, Military Academy Research Center, Department of Exact Sciences and Engineering, Portuguese Military Academy, Lisbon, Portugal*

⁴*UNESP – São Paulo State University, Campus of São João da Boa Vista, São João da Boa Vista, SP, Brazil*

*Corresponding author: elaine.cardoso@unesp.br

Highlights

- A predictive model for the HTC and maximum heat flux is developed;
- The developed model predicted well the database with an average error of <15%;
- The model is sensitive to the metal foam porosity, pore diameter, and thickness;
- The literature data that used dielectric fluid with metal foams were also predicted;
- The pore diameter can be determined by the PPI and porosity.

A NEW POOL BOILING HEAT TRANSFER MODEL FOR WETTING DIELECTRIC FLUIDS ON METAL FOAMS

Leonardo Lachi Manetti¹, Ana Sofia Oliveira Henriques Moita^{2,3} and Elaine Maria Cardoso^{1,4}

¹UNESP – São Paulo State University, School of Engineering, Post-Graduation Program in Mechanical Engineering, Av. Brasil, 56, 15385-000, Ilha Solteira, SP, Brazil

²IN+, Dep. Mechanical Engineering, Instituto Superior Técnico, Universidade de Lisboa, Lisbon, Portugal

³CINAMIL, Military Academy Research Center, Department of Exact Sciences and Engineering, Portuguese Military Academy, Lisbon, Portugal

⁴UNESP – São Paulo State University, Campus of São João da Boa Vista, São João da Boa Vista, SP, Brazil

*Corresponding author: elaine.cardoso@unesp.br

Highlights

- A predictive model for the HTC and maximum heat flux is developed;
- The developed model predicted well the database with an average error of <15%;
- The model is sensitive to the metal foam porosity, pore diameter, and thickness;
- The literature data that used dielectric fluid with metal foams were also predicted;
- The pore diameter can be determined by the PPI and porosity.

Abstract

Porous structures, as metal foams, can enhance the heat transfer performance. For a safe industrial application, a predictive model for both heat transfer coefficient and maximum heat flux is required. However, there is no correlation for dielectric fluids on metal foams available in the literature. This work aims to develop a semi-empirical model based on dimensional analysis for metal foam surfaces in pool boiling with different dielectric fluids. The model takes into account the porous heating surface characteristics (porosity, pore diameter, and thickness), the working fluid thermophysical properties, and its interaction. The model was developed based on the experimental database obtained by the authors and validated with the open literature database. Two metal foams with different characteristics were used for carrying out the pool boiling tests with two different working fluids: HFE-7100 and ethanol. The newly developed correlation predicted well the database with an average

error equal to 10.8% where 93.8% within the error range of $\pm 30\%$. To the maximum heat flux, the average error was 13.6% where 100% within the error range of $\pm 30\%$. The pore diameter and thickness play an important role in both models. The porosity and solid-phase thermal conductivity from the metal foam change the porous medium thermal conductivity, which influences the heat transfer coefficient (HTC). Finally, the properties of the working fluid also influence the predictive model, mainly the latent heat of vaporization, liquid thermal conductivity, and saturation temperature.

Keywords: pool boiling; metal foam; dielectric fluid; predictive model; immersion cooling.

Nomenclature

Alphabetic

a	cell diameter	[m]
A	Area	[m ²]
a_i	Multiple linear regression exponent	[-]
a_{sf}	Specific area	[m ² /m ³]
b_i	Multiple linear regression exponent	[-]
c_p	Specific heat capacity	[J/kg·K]
C_{sf}	Surface-fluid coefficient	[-]
d_f	Fiber diameter	[m]
d_p	Pore diameter	[m]
G	Shape factor, given by Eq. (39)	
h	Heat transfer coefficient	[W/m ² ·K]
h_{lv}	Latent heat of vaporization	[J/Kg]
Ja^*	Modified Jacob number	[-]
k	Thermal conductivity	[W/m·K]
k_{eff}	Effective thermal conductivity	[W/m·K]
k_M	Thermal conductivity from the porous medium given by Eq. (10)	[W/m·K]
L	Copper block distances	[m]
L_c	Characteristic length	[m]
m	Mass	[kg]
Nu	Nussel number	[-]
p	Pressure	[Pa]
p_{int}	Boiling chamber internal pressure	[Pa]
Pr	Prandtl number	[-]
Pr_{eff}	Effective Prandtl number	[-]
q''	Heat flux	[W/m ²]

q''_0	Reference heat flux	[W/m ²]
$q''_{measured}$	Heat flux measured at copper block	[W/m ²]
T	Temperature	[K]
u	Uncertainty	

Greek symbols

μ	Absolute viscosity	[kg/m·s]
γ	Ratio of the ligament node radii to the ligament length given by Eq. (28)	[-]
γ_{20}	Parcel of data predicted within an error band of ± 20	[-]
γ_{30}	Parcel of data predicted within an error band of ± 30	[-]
δ	Foam thickness	[m]
ΔT	Temperature difference	[K]
ε	Porosity	[-]
ξ	Dimensionless thickness	[-]
Π_k	Dimensionless number from Buckingham π theorem	[-]
ρ	Density	[kg/m ³]
ρ_r	Relative density	[-]
σ	Surface tension	[N/m]
Ψ	Dimensionless porosity	[-]
ω	Dimensionless PPI	[-]

Subscripts

1 to 4	Thermocouples position
atm	Atmospheric condition
calc	Calculated/predicted
circular	Circular heater cross-section
Cu	Copper property
exp	Experimental
foam	Metal foam property
l or liq	Saturated liquid fluid condition
max	Maximum point
Ni	Nickel property
s	Metal foam Solid-phase material
sat	Saturation fluid condition
sp	Sintered particle
square	Square heater cross-section
v or vap	Vapor saturated fluid condition
w	Surface wall

1. Introduction

Continuous improvement of the performance of instruments and equipment, mainly of electronics, supercomputers, and datacenters has led researchers to seek methods for cooling components with higher heat flux and heat density. Two-phase cooling systems have been widely studied for thermal management. Pool boiling is a low-cost technique due to the buoyancy of the bubbles, which creates a passive cooling without requiring pumping power or moving parts in the system [1–3]. It can be used in two configurations: indirect and direct immersion cooling; the former allows the use of many working fluids because there is an interface material between the heat source and the coolant; the latter eliminates the interface material and so increases the power density and energy efficiency in cooling high power electronics. However, the coolant must be dielectric [4–6]. Thus, although water possesses a higher boiling heat transfer coefficient, it is not compatible with electronic devices by using direct immersion cooling due to the problem of electrical short-circuit; on the other hand, dielectric fluids such as fluorochemical liquids are not electrically conductive and it has been proved to be highly suitable as a liquid medium for cooling [7]. However, these fluids have relatively poor thermophysical properties and extremely high wettability with most of the surfaces, which requires large superheat to initiate the boiling process - commonly referred to as ‘incipience excursion’ [8]. Therefore, to meet the cooling requirements of modern electronic devices by using dielectric fluids, the use of surface enhancement techniques have been widely applied to reduce boiling incipience superheat and improve both nucleate boiling heat transfer coefficient (HTC) and critical heat flux (CHF) - the highest heat flux in the nucleate boiling regime. According to Hendricks et al. [9], the heating surface can be modified by using three factors: (i) existence of random micro- or nano-size crevices and surface irregularities for bubble nucleation; (ii) porous surface structure that allows fluid inflow to keep nucleation sites active; and, (iii) surface protrusions that enlarge the boiling surface area. Porous surface structures have been widely reported to enhance heat transfer performance due to their interconnected porous, which increase the wetted area and the nucleation site density [10]. The porous thickness and pore size are the most important parameters of a porous surface, and their optimal values mainly depend on the fluid properties [11].

For a safe industrial application, a predictive model for both HTC and CHF is required. According to Wu et al. [12], mechanistic models and empirical or semi-empirical correlations have achieved some success in predicting boiling HTCs, mainly for smooth surfaces,

although some of them may predict experimental data well while failing for other data sets. The former is based on the heat flux partitioning model (RPI Model), which addresses various boiling heat transfer mechanisms calculated separately [13,14]. Generally, nucleate boiling is attributed to three heat transfer mechanisms: (1) natural convection in the region of the surface not influenced by the bubbles; (2) evaporation occurring during the bubble-growing period (a term related to the latent heat of evaporation); and, (3) so-called quenching due to the inflow of cold fluid on the heating surface and subsequent thermal boundary layer re-formation after bubble departure [15]. However, the mechanistic models require many parameters information, like bubble departure diameters and its frequencies, and active nucleation site densities. These parameters are difficult to obtain, especially the active nucleation site densities, which restricts the general validation of mechanistic models. Besides, the mechanistic models normally eliminate bubble interactions, and thus, they are not valid at high heat fluxes [16].

As a workaround, several authors proposed modeling nucleate boiling via dimensional analysis, avoiding the use of bubbles diameter, frequencies, and nucleation sites that must be obtained experimentally [17–20]. The empirical or semi-empirical correlations require critical analysis to find the main phenomena, properties, and dimensionless numbers to describe the pool boiling data set. The classical Rohsenow correlation [17] was developed based on a physical analogy between single-phase convection and nucleate boiling where Reynolds, Prandtl, and Stanton numbers are correlated [21]. Stephan and Abdelsalam [18] used regression analysis to derive the Nusselt number from other dimensionless variables. According to Stephan [22], the regression analysis showed that certain non-dimensional quantities prove to be important for some substances, but unimportant for others. A disadvantage of these correlations is the fact that the composition of the heating surface has not been taken into consideration. Some of them address the effect of surface topography by considering the surface roughness; however, this parameter is not representative of the geometric features of the surface pattern and so it is weakly correlated with the quantities describing nucleation and bubble dynamics [19].

Teodori et al. [19] proposed a new correlation based on an empirical method to predict the pool boiling HTC on regular micro-patterned heating surfaces. Two correlations were obtained by dimensional analysis, which was slightly different in terms of the phenomenological description of the boiling process. Both of them were able to predict the heat transfer coefficient within an error of $\pm 30\%$. Also, these correlations could predict fluids behavior with significantly different thermophysical properties. Recently, Liang et al. [23]

studied pool boiling enhancement on micro-pit surfaces by using water as the working fluid; to predict the data, they modified the Rohsenow correlation [17] by incorporating the pit depth. The correlation showed a good agreement with the experimental data, especially in the nucleate boiling region with relatively high HTC. On the other hand, for the relatively low HTCs, partial data deviate slightly from the 20% error line due to the single-phase HTCs included in the database. Despite this, the correlation estimated the HTC prior to CHF, with a mean absolute percentage error (MAPE) of 8.3%. However, according to Lin and Kedzierski [11], the boiling models for the structured surface are not directly applicable to the porous surface due to the randomness of the porous surface geometry (it is more difficult to develop a mechanistically based model for the boiling heat transfer on a porous surface); consequently, few studies predicting the heat transfer on porous surfaces were found in the open literature.

Nishikawa and Ito [24] developed an empirical correlation based on their pool boiling data of R-11, R-113, and benzene at saturation temperature and atmospheric pressure on the porous surfaces coated by copper or bronze particles, whose diameter ranged from 100 to 1000 μm . The correlation incorporates the effects of porosity – ranged from 0.38 to 0.71 – and thickness of the coating layer – ranged from 0.5 to 5 mm, particle diameter, and fluid properties. Xu et al. [25] used Rohsenow correlation [17] to determine the correlation for a highly porous surface – metal foams – by adding a modification factor and exponent. The effects of pore density, porosity, and thickness were included in the modified factor and exponent. For water pool boiling heat transfer, approximately 80% of the predicted data were within an error band of $\pm 30\%$. Besides, Righetti et al. [26] modified an exponent from Xu et al. [25] model to predict the boiling of water on thicker aluminum foams and obtained an absolute deviation of 12.1%. Recently, Hu et al. [27] also developed a correlation based on the Rohsenow correlation [17] by introducing a metal foam influence factor. They incorporated the effect of area density, pore density, porosity, and advancing contact angle. Besides, they used their database with boiling of water on uncoated and hydrophobic metal foam covers and data from Shi et al. [28] and Xu et al. [29] for fitting the coefficients. The predicted values of the new correlation agreed with 95% of the experimental data within a deviation of $\pm 20\%$, and the average deviation was 10.2%

Based on the literature review, immersion cooling with porous heating surfaces has the potential for industrial applications but, before this, it is advisable to determine the pool boiling heat transfer performance. Correlations obtained from the dimensional analysis are more suitable for the entire nucleate boiling curve. As reported, some researchers focus on

correlations by using refrigerant fluids with a sintered porous layer while others by using water on metal foams; but until now, there is no correlation for dielectric fluids on metal foams. Moreover, the predictive model should be validated with a database from literature, *i.e.*, data that were not used in the coefficients/exponent regression to test the model and avoid overfitting [30].

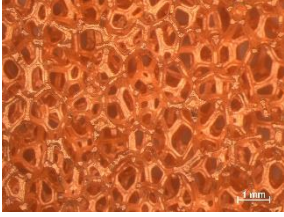
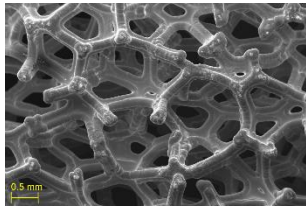

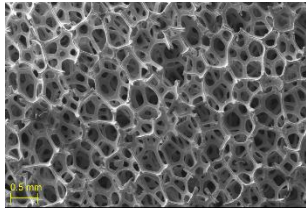
In this way, this work aims to develop a semi-empirical correlation, based on dimensional analysis, for metal foams surfaces in pool boiling with a dielectric fluid, taking into account the porous heating surface characteristics (porosity, pore diameter, and thickness), the working fluid thermophysical properties, and the interaction between them. The correlation is developed based on our experimental database and validated with the open literature database.

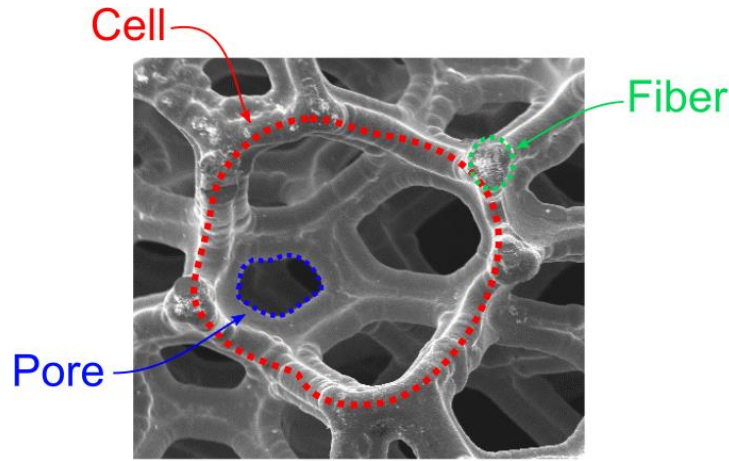
2. Experimental setup and foams samples

2.1 Foams parameter

Two metal foams with different parameters were used for carrying out the pool boiling tests, namely a copper foam (Cu foam), and nickel foam (Ni foam). **Table 1** shows the SteREO and SEM images from each one; they are open-cell metal foams (**Figure 1**) fabricated by using the metal deposition process as detailed by Ashby et al. [31] and Banhart [32]. They were acquired from Nanoshel® in $500 \times 500 \text{ mm}^2$ panels with 3 mm thick. To use the foam in pool boiling tests, they were cut in a square section of $16 \times 16 \text{ mm}^2$ by using a wire electrical discharge machining (wire-EDM). After, to perform the PPI measurements by using the images, seven lines in each direction – horizontal and vertical, were traced and the number of porous intercepted by the lines was counted; so, an average yields the PPI of the open-cell metal foam. For Cu and Ni open-cell metal foam, the average PPI values were 31.75 ± 6.2 and 62.72 ± 12.85 , respectively.

Table 1. Metal foams images from SteREO and SEM microscopy.

Foam	SteREO image	SEM image
Cu		
Ni		

**Figure 1.** Open-cell foam structure.

The metal foams porosity (ε) was obtained by weighing samples of the same size in a precision balance and comparing the foam density, $\rho_{\text{foam}} = m_{\text{foam}}/V_{\text{foam}}$, with the solid density,

$$\varepsilon = 1 - \rho_r = 1 - \frac{\rho_{\text{foam}}}{\rho_s} \quad (1)$$

Also, X-ray microcomputed tomography (μ CT) images were taken from a Skycan 1272 at a resolution of 15 μm (100 kV X-ray source voltage) to precisely characterize the foam granulometry - cell, porous, and fibers diameters (a , d_p and d_f , respectively) as shown in **Figure 1**. First, the μ CT virtual slices were input in the iMoph software [33] and the gray-level threshold value was selected such that the porosity of the reconstructed 3D volume matched with the measured foam porosity (**Table 2**); next, iMorph uses the ‘marching cubes’ algorithm to extract the interface between the porous and solid phases by creating a

triangulated surface mesh that is rendered to form a solid. Finally, cells were individualized (represented by a color) by using cell segmentation that was obtained after maximal ball identification and watershed transform [34,35]. The pores (throat) are the contact region between two individualized cells that can be observed after the cell extraction. Therefore, the cell diameter and fibers diameters were obtained from the maximal ball identification and the pore diameter was obtained from the area of cell contacts by considering the diameter of a circle. **Figure 2** shows a process flowchart from the steps in iMorph and **Table 2** shows the average and standard deviation of the porosity (ε), cell diameter (a), pore diameter (d_p), and fiber diameter (d_f) for each foam.

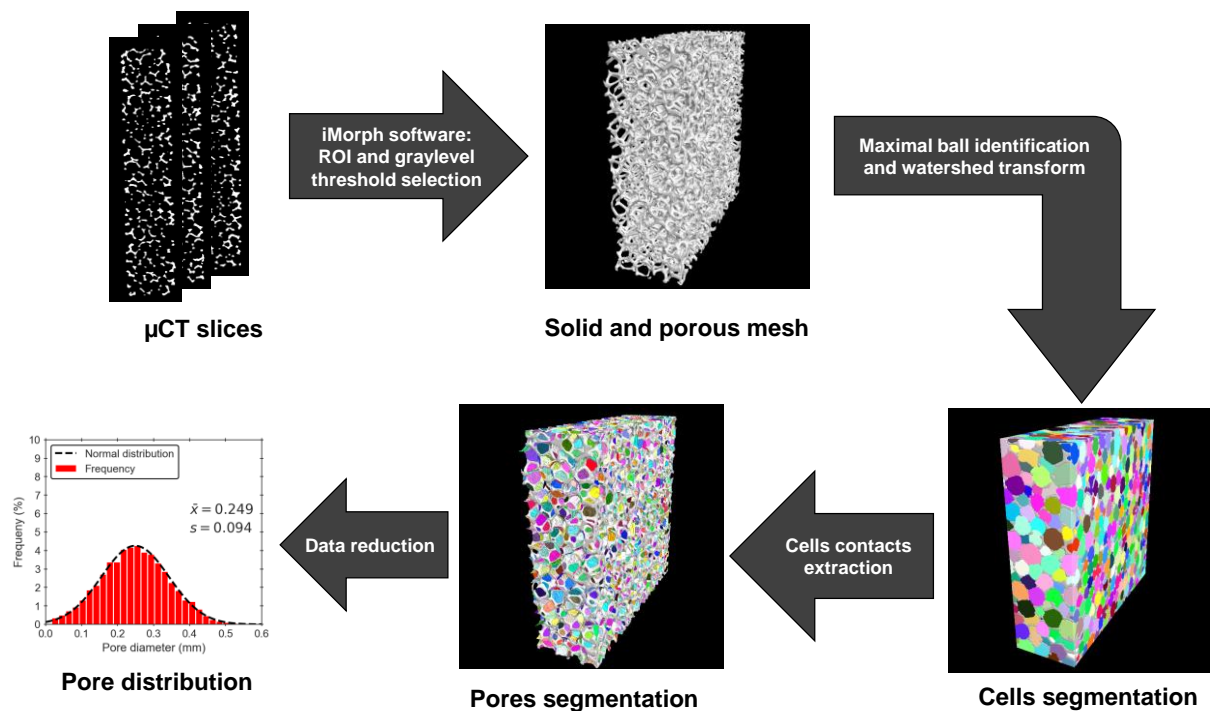


Figure 2. Steps of the foam granulometry characterization by using iMorph.

Table 2. Metals foams characteristics.

Foam	$m_{\text{foam}} \times 10^3$ (kg)	ρ_{foam} (kg/m ³)	ρ_r (%)	ε (%)	a (mm)	d_p (mm)	d_f (mm)
Cu	0.697 ± 0.022	908.1 ± 28.63	10.0 ± 0.32	90.0 ± 0.32	1.08 ± 0.24	0.46 ± 0.25	0.13 ± 0.04
Ni	0.106 ± 0.010	138.0 ± 14.12	1.6 ± 0.15	98.4 ± 0.15	0.46 ± 0.10	0.25 ± 0.09	0.07 ± 0.02

¹Solid density: $\rho_{\text{Cu}} = 8960 \text{ kg/m}^3$; $\rho_{\text{Ni}} = 8900 \text{ kg/m}^3$ [36].

The metal foams with the original thickness were soldered on the copper block with a plain and square plate on the upper surface ($16 \times 16 \text{ mm}^2$) of the copper cylinder (**Figure 3**). Furthermore, other foam thicknesses were used in this work. The thickness level variation

was carried out by using the electric discharge machining process (EDM) as explained by Manetti et al. [37]. Three different thickness (δ) was tested for the copper foam (3 mm, 2 mm, and 1 mm) while four different thickness was tested for the nickel foam (3 mm, 2 mm, 1 mm, 0.5 mm). The last thickness for both foams is relative to the cell mean diameter, *i.e.*, the lowest thickness must be close to the cell diameter in order to not mischaracterize the foam geometry.

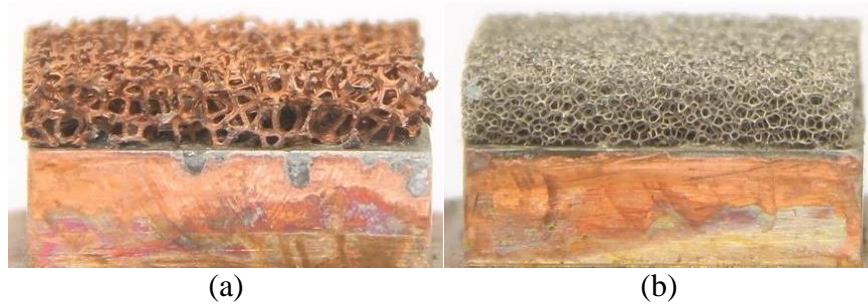


Figure 3. Metal foam ($\delta = 3$ mm) soldered on the plain surface: (a) Cu foam; and (b) Ni foam.

2.2 Pool boiling experimental facilities

The database for developing the new correlation was obtained by boiling two different working fluids: HFE-7100 and ethanol (both dielectric) on the metal foams previously described. Moreover, the experimental tests were carried out in two different research laboratories with different facilities by using a similar methodology. First, pool boiling of HFE-7100 (at local atmospheric pressure) on the metal foams were carried out at the School of Engineering (UNESP, Brazil). Next, pool boiling of ethanol (at local atmospheric pressure) on the metal foams were carried out at the IN+ (IST, Portugal). The following subsections describe both facilities.

2.2.1 HFE-7100 pool boiling facility and data reduction

The pool boiling tests by using HFE-7100 were performed in the apparatus in **Figure 4** and **Figure 5**, which consists of a boiling chamber with a rectangular glass section (120×100 mm²) with a thickness of 5 mm and 200 mm height. A thermal bath was used to control the internal condenser coil temperature located at the top of the boiling chamber. An auxiliary heater, controlled with a variable transformer (VARIAC), submerged in the working fluid was used to degas the fluid before the beginning of each test and maintain the liquid

temperature near the saturation point during the test. Two K-type thermocouples, T_{liq} , and T_{vap} , located in the working fluid and vapor, respectively, allowed monitoring the test condition temperature. The pressure inside the boiling chamber was measured by a pressure transducer and maintained close to the local atmospheric pressure, $p_{\text{atm}} = 98 \text{ kPa}$, during the boiling tests.

Three K-type thermocouples (T_1 , T_2 , and T_3) with 0.5 mm diameters were used to measure the heat flux (q''_{measured}) and estimate the wall temperature (T_w). A cartridge resistance heated the bottom part of the copper block; the power was supplied by a stabilized variable DC power source. The thermal insulation of the test section consisted of polytetrafluoroethylene (PTFE). A data acquisition system (Agilent 34970A) was used to acquire all the data signals (power, pressure, and temperature) and, then, they were registered in a personal computer using the Agilent Benchlink Data Logger. The heating effect was imposed by increasing the electrical power according to heat flux steps until a condition close to the CHF. For each metal foam test, the experiment was carried out at least twice under similar conditions to ensure that the results were repeatable. More details about the experimental setup and data reduction of that subsection can be found in Manetti et al. [37,38].

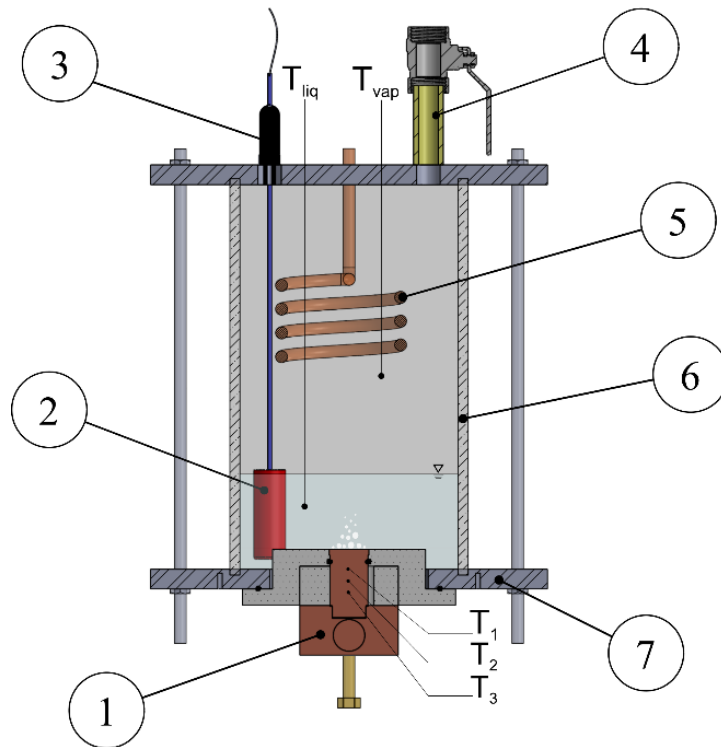


Figure 4. Pool boiling chamber for HFE-7100 boiling: (1) copper block; (2) auxiliary heater; (3) pressure transducer; (4) vacuum/feed valve; (5) condenser; (6) glass chamber; (7) stainless steel plate.

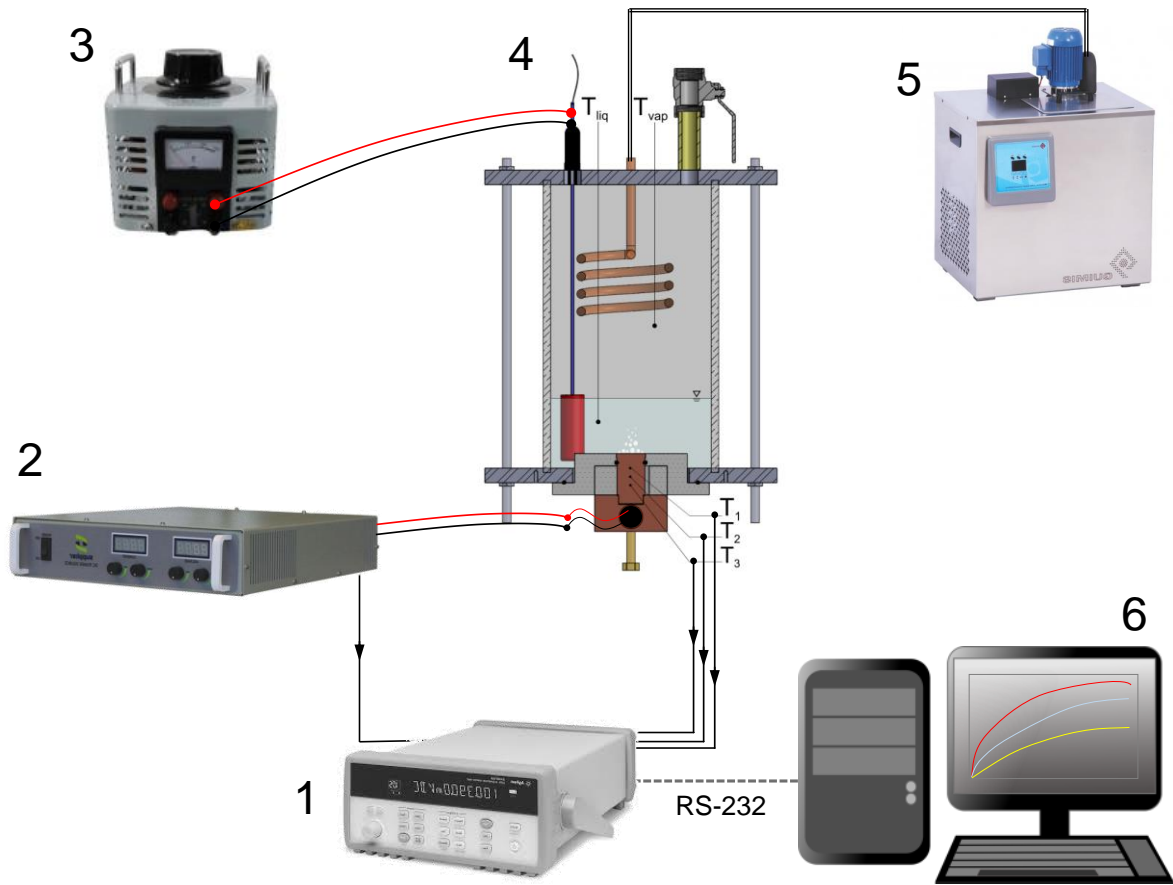


Figure 5. Schematic of the experimental facility: (1) Data acquisition; (2) DC power source; (3) VARIAC; (4) Pool boiling chamber; (5) thermal bath; (6) Datalogger/Computer.

2.2.2 Ethanol pool boiling facility and data reduction

The pool boiling tests by using ethanol were performed in the apparatus in **Figure 6** and **Figure 7**. The boiling chamber was projected to be heated by Joule effect in a stainless-steel foil as presented by Pontes et al. [39,40]; however, it was modified to a copper block heating for this work. The core component is a cylindrical metallic tank with three glass windows for visualization. The upper part is closed with a rectangular flange where an absolute pressure transducer (0 – 2 bar) is located, together with two K-type thermocouples, T_{liq} , and T_{vap} , a valve for filling the chamber, and a connection to an external condenser. Ethanol is maintained at the saturation temperature with the aid of an auxiliary cartridge heater fed by a VARIAC transformer and the pressure inside the boiling chamber was maintained close to the local atmospheric pressure, $p_{atm} = 100.5$ kPa, during the boiling tests. The lower part is closed with a circular flange where the test section is coupled. The test section consists firstly of the main cartridge heater fed by another VARIAC transformer; next, a copper block was used to measure the heat flux; finally, the heating surface is located at the top. The thermal

insulation in the radial and axial direction of the test section consisted of PTFE. Moreover, to decrease the contact resistance between the copper block and the heating surface, a thermal paste (arctic mx-2) was applied.

Three K-type thermocouples (T_2 , T_3 , and T_4) with 0.5 mm diameters were used to measure the heat flux (q''_{measured}) in the copper block and a fourth one (T_1), located on the heating surface after the contact resistance, was used to estimate the wall temperature (T_w). A data acquisition system (Data Translation® DT9828) was used to acquire the data signals from the thermocouples, a National Instruments® BNC-2120 acquired the signal from the pressure transducer and a digital multimeter Tektronix® DMM 4020 measured the power applied. Then, all signals were registered in a personal computer using a LabView routine.

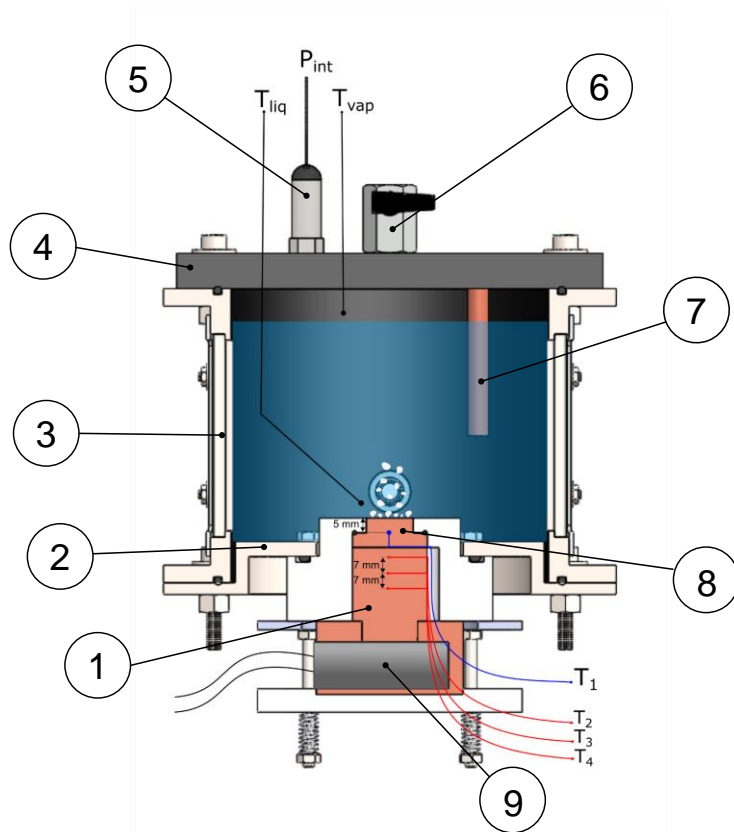


Figure 6. Pool boiling chamber for ethanol boiling: (1) cooper block; (2) lower flange; (3) tank with windows; (4) upper flange; (5) pressure transducer; (6) vacuum/feed valve and connection to the condenser; (7) auxiliary heater; (8) heating surface (9) main heater.

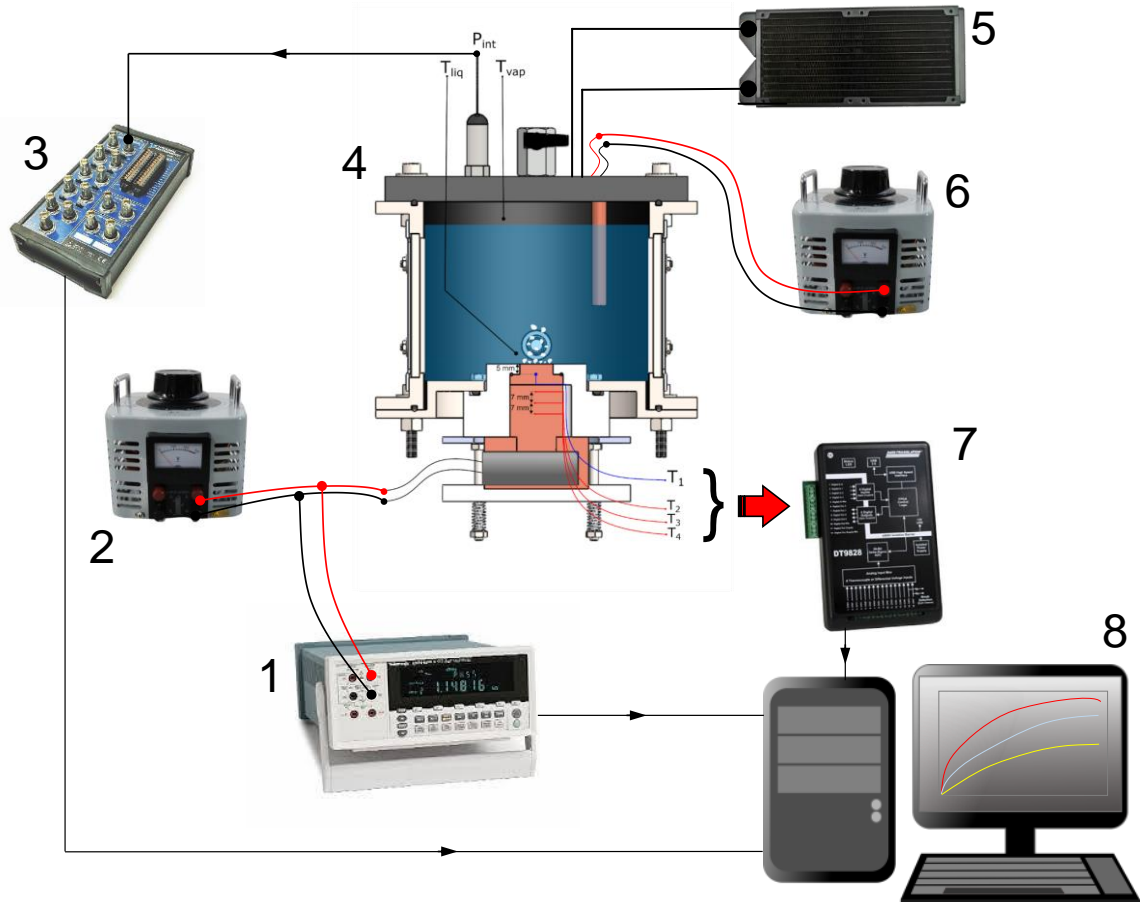


Figure 7. Schematic of the experimental facility: (1) Digital multimeter; (2) VARIAC to the main heater; (3) Data acquisition to pressure transducer; (4) Pool boiling chamber; (5) external condenser; (6) VARIAC to auxiliary heater; (7) Data acquisition to thermocouples; (8) Datalogger/Computer.

Before the boiling tests, a vacuum was created in the tank to feed it with ethanol. After feeding, the auxiliary heater boiled the working fluid for 1 hour for degassing it. So, the heating effect was imposed by increasing the electrical power according to heat flux steps, starting close to 35 kW/m^2 , until a condition close to the CHF, characterized by the non-stability of the heating surface temperature. For each metal foam test, the experiment was carried out at least twice, under similar conditions, to ensure that the results were repeatable.

The heat flux was measured between the three first thermocouples, where the middle one was used just to confirm the linear temperature profile [37]. So, the measured heat flux by using Fourier's law of conduction through the more spaced thermocouples in the copper metering block was calculated,

$$q''_{\text{measured}} = \frac{A_{\text{circular}}}{A_{\text{square}}} \cdot k_{\text{Cu}} \cdot \frac{\Delta T_{24}}{L_{24}} \quad (2)$$

where the area ratio is due to the square cross-section ($16 \times 16 \text{ mm}^2$) at the surface upper level and the circular area of the copper block (25 mm in diameter) at the lower level; L_{24} is the thermocouples distance equal to 14 mm as shown in **Figure 6**.

The HTC was calculated using Newton's law of cooling given by:

$$\text{HTC}_{\text{exp}} = \frac{q''_{\text{measured}}}{T_w - T_{\text{sat}}(p_{\text{int}})} = \frac{q''_{\text{measured}}}{\Delta T_{\text{sat}}} \quad (3)$$

where $T_{\text{sat}}(p_{\text{int}})$ corresponds to the saturation temperature of the ethanol, at pressure inside de boiling chamber and T_w is the wall temperature given as follows:

$$T_w = T_1 - \frac{q''_{\text{measured}}}{k_{\text{Cu}}} L_{1w} \quad (4)$$

where the second term is the linear temperature profile in the square section ($L_{\text{sw}} = 5 \text{ mm}$), as shown in **Figure 6**.

The experimental uncertainties (u) were calculated by using the method described by Moffat [41] where the uncertainty in the result R is a function of the independent variables X_i as follow:

$$u_R = \left[\left(\sum_i^n \frac{\partial R}{\partial X_i} u_{X_i} \right)^2 \right]^{\frac{1}{2}} \quad (5)$$

Therefore, the relative uncertainty for the heat flux between the thermocouples 4 and 2 was given by:

$$\frac{u_{q''_{\text{measured}}}}{q''_{\text{measured}}} = \left[\left(\frac{u_{\Delta T_{42}}}{\Delta T_{42}} \right)^2 + \left(\frac{u_{L_{42}}}{L_{42}} \right)^2 \right]^{1/2} \quad (6)$$

where the differential uncertainty of the K-type thermocouples, $u_{\Delta T}$, was $\pm 0.3 \text{ }^\circ\text{C}$ (corresponds to the thermocouples uncertainties after the calibration); the uncertainty in the position of the thermocouple junction was estimated to be $\pm 0.03 \text{ mm}$, and the wall superheat uncertainty was given by:

$$u_{\Delta T_{\text{sat}}} = \left[(u_{\Delta T})^2 + \left(-\frac{L_{1w}}{k_{\text{Cu}}} u_{q''_{\text{measured}}} \right)^2 + \left(-\frac{q''_{\text{measured}}}{k_{\text{Cu}}} u_{L_{1w}} \right)^2 \right]^{1/2} \quad (7)$$

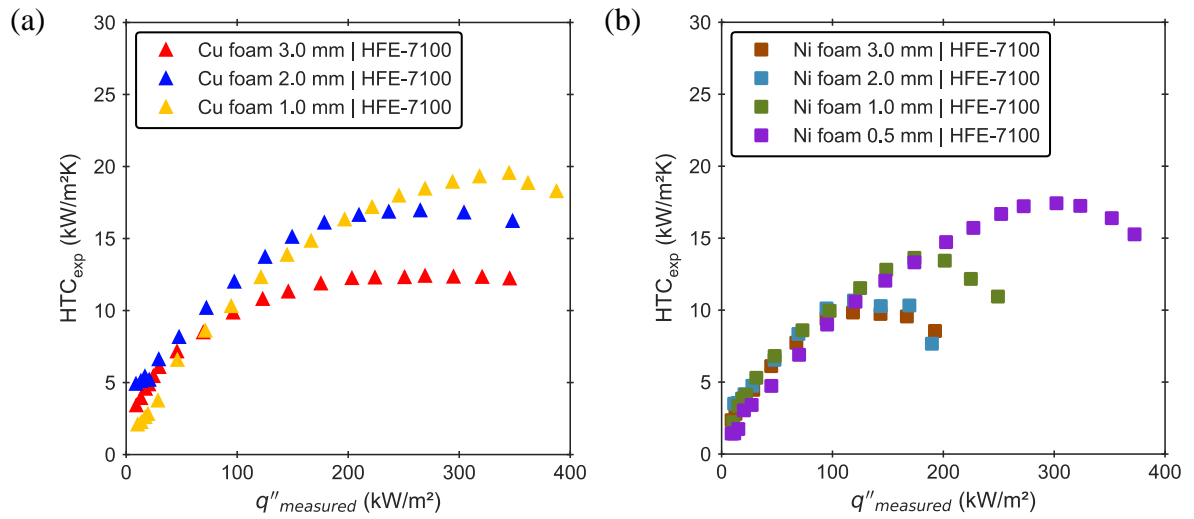
Finally, the HTC uncertainty was given by:

$$\frac{u_h}{h} = \left[\left(\frac{u_{\Delta T_{\text{sat}}}}{\Delta T_{\text{sat}}} \right)^2 + \left(\frac{u_{q''_{\text{measured}}}}{q''_{\text{measured}}} \right)^2 \right]^{1/2} \quad (8)$$

Therefore, the experimental uncertainty of the heat transfer coefficient is higher in low heat fluxes while it decreases as heat fluxes are increased.

3. Database

The first run of the experimental database – HTC for both metal foams: Cu and Ni; and, both fluids, HFE-7100 and Ethanol – are presented in **Figure 8**.



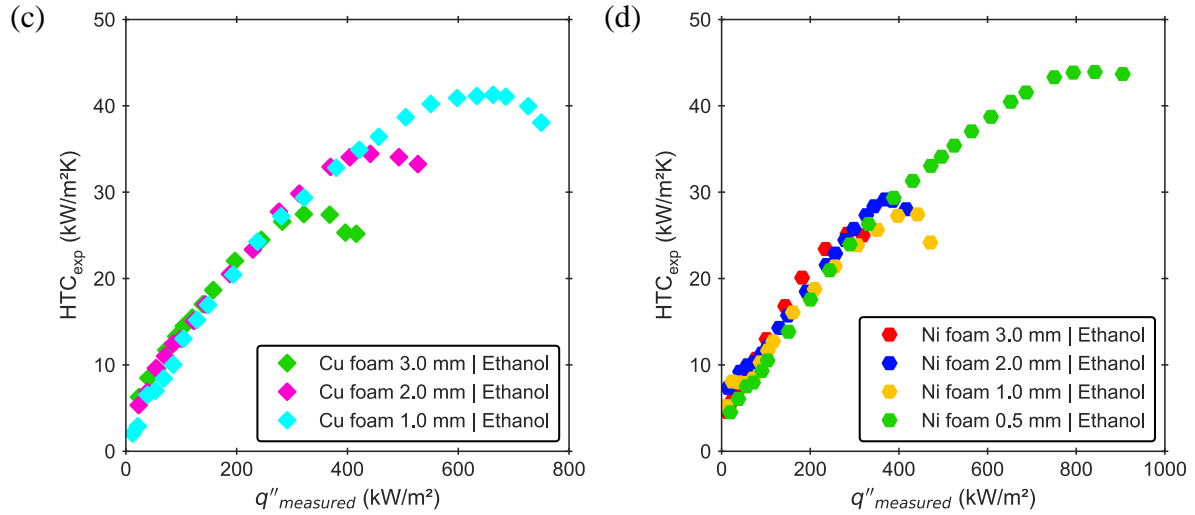


Figure 8. HTC curves of metal foam with different thickness and fluids: (a) HFE-7100 on Cu foams ($\delta = 1$ to 3 mm); (b) HFE-7100 on Ni foams ($\delta = 0.5$ to 3 mm); (c) Ethanol on Cu foams ($\delta = 1$ to 3 mm); (d) Ethanol on Ni foams ($\delta = 0.5$ to 3 mm).

One may observe in **Figure 8** that the thickness level variation plays an important role in the boiling curves. Higher thickness has a greater wetted area, which can improve the heat transfer at the first heat fluxes while some nucleation sites are activated and other regions stayed on natural convection. As the heat flux increases, more vapor bubbles emerge from the foam structure and the boiling regimes change to fully developed nucleate boiling. In this range of heat fluxes, there is a competition of the convection area (wetted area) and vapor bubble flow resistance to outlet the foam structure. Therefore, for each heat fluxes range, there is an optimum thickness as showed by Manetti et al. [37].

Another parameter on the foam heat transfer phenomenon is the pore diameter, which is correlated to the specific area (area density) as reported by Calmidi and Mahajan [42]; a lower pore diameter can result in a better heat transfer performance at low heat fluxes; however, with high thickness, it could increase the vapor bubble flow resistance decreasing the HTC. So, the thicker and smaller the pore, the larger the liquid-vapor counter-flow, since the liquid replenishment is inhibited, leading to a lower heat transfer coefficient and an earlier occurrence of dryout - defined as the condition at which the HTC presents a maximum value [38].

In addition, the foam material properties, specifically the thermal conductivity, k_s , also play an important role in the thermal behavior; the higher the thermal conductivity of the foam material the higher the effective foam thermal conductivity and, consequently, the higher the foaming efficiency (fin efficiency) as reported by Manetti et al. [38].

Finally, the fluid thermophysical properties influence the HTC; the higher the fluid thermal conductivity and the latent heat of vaporization, the higher the HTC.

3.1 Prediction of the Experimental Database by Using Known Correlations

As cited in the Introduction Section, Nishikawa and Ito [24] correlated their data to predict the Nusselt number as follow:

$$Nu = \frac{h \cdot \delta}{k_M} = 1 \times 10^{-3} \left(\frac{\sigma^2 h_{lv}}{q''^2 \delta^2} \right)^{0.0284} \left(\frac{\delta}{d_{sp}} \right)^{0.560} \left(\frac{q'' d_{sp}}{\varepsilon h_{lv} \mu_v} \right)^{0.593} \left(\frac{k_M}{k_l} \right)^{-0.708} \left(\frac{\rho_l}{\rho_v} \right)^{1.67} \quad (9)$$

where σ , h_{lv} , k_l , ρ_l , ρ_v , and μ_v represent the fluid thermophysical properties: surface tension [N/m], latent heat of vaporization [J/kg], thermal conductivity [W/m.K], liquid and vapor density [kg/m³], and dynamic viscosity [kg/m.s], respectively. Besides, d_{sp} represents the sintered particle diameter (solid phase of the porous medium) and k_M is the thermal conductivity of the porous medium given by the parallel model:

$$k_M = \varepsilon k_l + (1 - \varepsilon) k_s \quad (10)$$

To evaluate the capability of the previous correlation to predict HTC results for pool boiling, the current experimental database was compared with the values given by Eq. (10) (calculated Nusselt). Thus, to apply our database in Nishikawa and Ito [24] correlation, we changed d_{sp} to the foam fiber diameter, d_f , because they are both the solid phase of the porous medium. In addition, the data after the highest HTC of each curve, **Figure 8**, was removed because the predictive model does not consider the dryout phenomenon. **Figure 9** shows the calculated Nusselt number by the previous correlation *versus* the experimental database. Also, **Table 3** presents the statistical analysis between experimental and predicted data, including the parcel of data predicted within an error band of $\pm 20\%$, γ_{20} , and $\pm 30\%$, γ_{30} ; and, the mean average percentage error, MAPE, defined as follows:

$$MAPE = \frac{\sum_{i=1}^N \left| \frac{Nu_{calc} - Nu_{exp}}{Nu_{exp}} \right|}{N} \quad (11)$$

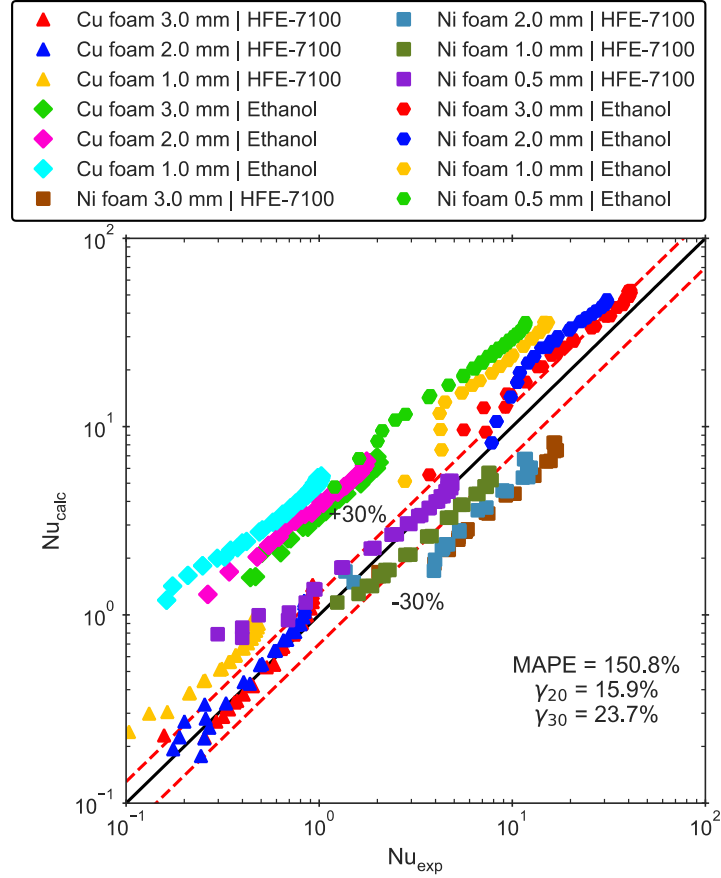


Figure 9. Comparison between Nusselt number from the experimental database and Nusselt number calculated by Nishikawa and Ito [24] correlation.

Table 3. Statistical analysis between experimental and predicted data from the Nishikawa and Ito [24] correlation.

Surface	Fluid	MAPE	γ_{20}	γ_{30}
Cu foam 3.0 mm	HFE-7100	20.0%	60.6%	72.7%
Cu foam 2.0 mm	HFE-7100	16.7%	71.4%	82.1%
Cu foam 1.0 mm	HFE-7100	101.8%	0.0%	0.0%
Cu foam 3.0 mm	Ethanol	241.8%	0.0%	0.0%
Cu foam 2.0 mm	Ethanol	299.9%	0.0%	0.0%
Cu foam 1.0 mm	Ethanol	550.3%	0.0%	0.0%
Ni foam 3.0 mm	HFE-7100	51.9%	5.0%	5.0%
Ni foam 2.0 mm	HFE-7100	45.5%	5.0%	10.0%
Ni foam 1.0 mm	HFE-7100	26.9%	12.5%	62.5%
Ni foam 0.5 mm	HFE-7100	26.3%	63.6%	66.7%
Ni foam 3.0 mm	Ethanol	38.7%	3.4%	41.4%
Ni foam 2.0 mm	Ethanol	57.1%	5.6%	11.1%
Ni foam 1.0 mm	Ethanol	140.4%	0.0%	0.0%
Ni foam 0.5 mm	Ethanol	241.3%	0.0%	0.0%

As can be seen, the Nishikawa and Ito [24] correlation over predicted most of the database. It is expected that the experimental database does not fit well with the Nishikawa and Ito [24] correlation mainly due to the surface characteristics. The sintered particle layer tested by Nishikawa and Ito [24] had a porosity range from 0.38 to 0.71 while our metal foams samples are from 0.9 to 0.98. Moreover, the particle layer had a higher particle diameter than the metal foam fiber diameter.

Another model tested was from Xu et al. [25] modified by Righetti et al. [26] as follow:

$$\frac{q''}{\mu_l h_{lv}} \sqrt{\frac{\sigma}{g(\rho_l - \rho_v)}} = c \left(\frac{c_{p,l} \Delta T_{sat}}{C_{sf} h_{lv} Pr_l} \right)^b \quad (12)$$

where b and c are parameters fitted by Righetti et al. [26],

$$b = 1.53\psi^{-0.5124}\omega^{0.01926}\xi^{0.1793} \quad (13)$$

$$c = \begin{cases} 10^{(5.5949\psi^{-0.2323}\omega^{0.003588}\xi^{0.025}-5.506)}, & 0 < q'' \leq 250 \text{ kW/m}^2 \\ 10^{(5.5949\psi^{-0.2323}\omega^{0.003588}\xi^{0.025}-5.4059)}, & 250 < q'' \leq 490 \text{ kW/m}^2 \\ 10^{(5.5949\psi^{-0.2323}\omega^{0.003588}\xi^{0.025}-5.3089)}, & 490 < q'' \leq 1460 \text{ kW/m}^2 \end{cases} \quad (14)$$

and, $\omega = \text{PPI}/5$; $\xi = \delta/5 \text{ mm}$; $\Psi = \varepsilon/0.9$; and, $C_{sf} = 0.0165$.

Figure 10 shows the Eq. (12) left-hand, *i.e.*, the calculated heat flux *versus* the experimental database. Also, **Table 4** presents the statistical analysis between experimental and predicted data.

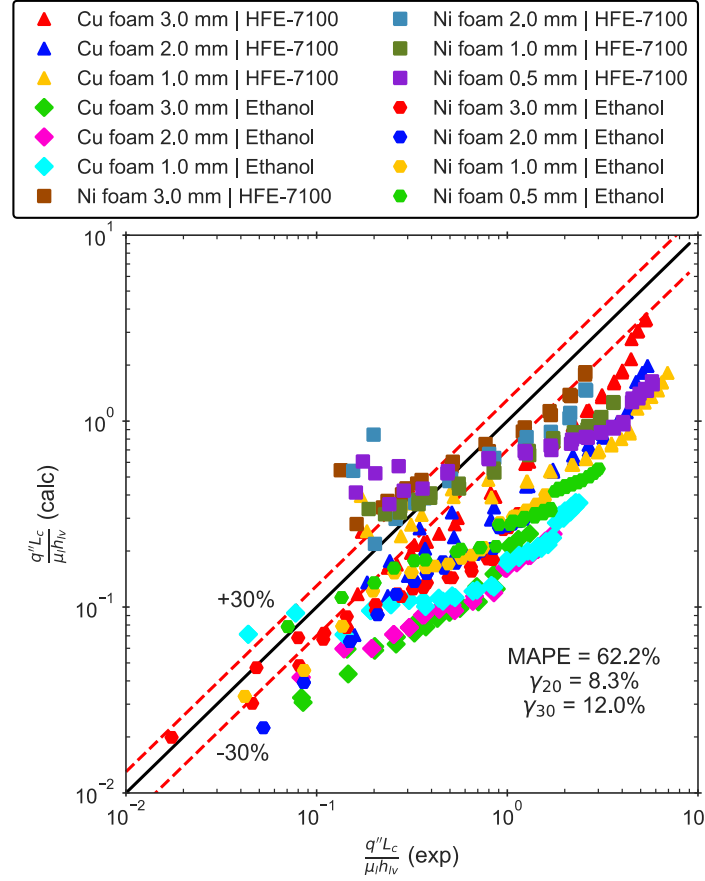


Figure 10. Eq. (12) left-hand comparison between the experimental database and those calculated by the model from Xu et al. [25] modified by Righetti et al. [26].

Table 4. Statistical analysis between experimental and predicted data from the Xu et al. [25] model modified by Righetti et al. [26].

Surface	Fluid	MAPE	γ_{20}	γ_{30}
Cu foam 3.0 mm	HFE-7100	46.7%	0.0%	3.0%
Cu foam 2.0 mm	HFE-7100	60.2%	0.0%	10.7%
Cu foam 1.0 mm	HFE-7100	60.9%	16.7%	19.4%
Cu foam 3.0 mm	Ethanol	76.7%	0.0%	0.0%
Cu foam 2.0 mm	Ethanol	77.0%	0.0%	0.0%
Cu foam 1.0 mm	Ethanol	73.4%	4.8%	4.8%
Ni foam 3.0 mm	HFE-7100	47.6%	20.0%	35.0%
Ni foam 2.0 mm	HFE-7100	52.0%	45.0%	50.0%
Ni foam 1.0 mm	HFE-7100	42.3%	25.0%	33.3%
Ni foam 0.5 mm	HFE-7100	71.1%	6.1%	15.2%
Ni foam 3.0 mm	Ethanol	56.2%	10.3%	10.3%
Ni foam 2.0 mm	Ethanol	66.2%	0.0%	0.0%
Ni foam 1.0 mm	Ethanol	58.0%	0.0%	6.5%
Ni foam 0.5 mm	Ethanol	65.1%	8.9%	8.9%

Unlike the Nishikawa and Ito [24] correlation, the Xu et al. [25] the model modified by Righetti et al. [26] under predicted our experimental data. It is because the data used to develop the model was based on water pool boiling tests, which has wettability and thermophysical properties higher than the dielectric fluids tested in the current work.

4. Results and Discussion

4.1 New HTC Predictive Model Formulation

The newly developed correlation was obtained based on the Buckingham π theorem [43] to formulate the independent fundamentals physics dimensions, r , chosen to represent the dependent parameters. The application of this theorem first requires a decision on which of the parameters play roles on the boiling HTC (h) of wetting dielectric fluids on metal foams:

- first, the boiling HTC is dependent on the heat flux, q'' . Note that the heat flux is the imposed variable; thus, the wall superheating (ΔT_{sat}) must not be chosen to avoid redundancy.
- next, as previously mentioned, the boiling HTC on metal foams is a function of surface characteristics; thus, the proposed correlation takes into account the effect of foam thickness (δ), pore diameter (d_p) and porous medium thermal conductivity or effective thermal conductivity (k_{eff}).
- moreover, the fluid thermophysical properties such as the saturation temperature, T_{sat} ; the characteristic length (capillary length), L_c ; the latent heat of vaporization, h_{lv} ; specific heat of the liquid, $c_{p,l}$; and dynamic viscosity of the liquid, μ_l ; also, are important parameters for the HTC predictive model.

Finally, the following functional relation can be written:

$$h = f(q'', L_c, k_{\text{eff}}, c_{p,l}, T_{\text{sat}}, \mu_l, h_{lv}, \delta, d_p) \quad (15)$$

The $n = 10$ variables are listed in the dimension $\text{MLT}\Theta$ [44] that implies in $r = j = 4$ repeating variables ($q'', L_c, k_{\text{eff}}, c_{p,l}$) resulting in $k = n - j = 6$ dimensionless variables (Π_k).

The first dimensionless number obtained is the Nusselt number,

$$\Pi_1 = \text{Nu} = \frac{h \cdot L_c}{k_{\text{eff}}} \quad (16)$$

which is similar to the Nusselt number obtained by Teodori et al. [19] and Kiyomura et al. [20]; however, it incorporates the effective thermal conductivity from the porous medium as Nishikawa and Ito [24] correlation.

The second dimensionless number,

$$\Pi_2 = \frac{q'' \cdot L_c}{k_{\text{eff}} T_{\text{sat}}} \quad (17)$$

is the only one where the imposed variable, q'' , appears. That dimensionless number is associated with the effect of liquid agitation near the wall. A similar dimensionless number was obtained by Stephan and Abdelsalam[18] and Teodori et al. [19].

The third dimensionless number is a porous media Prandtl number [45,46], or also called of effective Prandtl number [47] because it incorporates the effective thermal conductivity from the porous media as follow:

$$\Pi_3 = \text{Pr}_{\text{eff}} = \frac{c_{p,l} \mu_l}{k_{\text{eff}}} \quad (18)$$

The effective Prandtl number is important because the heat transfer occurs directly from the porous heating surface to the adjacent liquid, adapting a single-phase forced convection heat transfer model to nucleate pool boiling. As reported by Gerardi et al. [14], Thiagarajan et al. [15], and Teodori et al. [19], the quenching effect, *i.e.*, the heat transfer due to the re-formation of the thermal boundary layer, plays an important role on the nucleate boiling heat transfer.

The fourth dimensionless number is the modified Jakob number, which accounts the sensible heat and the latent heat of vaporization – one of the most relevant property for phase-change heat transfer, as follow:

$$\Pi_4 = \text{Ja}^* = \frac{c_{p,l} T_{\text{sat}}}{h_{lv}} \quad (19)$$

where the wall superheating was changed by the saturation temperature to avoid two imposed variables in the same model, as previously described.

Up to now, the foam properties only appear in the effective thermal conductivity. The following numbers take into account the characteristic dimension of the metal foam; the effect of the thickness,

$$\Pi_5 = \frac{\delta}{L_c} \quad (20)$$

which is important due to the effect of thickness in the HTC, as shown in **Figure 8**. Also, the effect of the pore diameter,

$$\Pi_6 = \frac{d_p}{L_c} \quad (21)$$

These dimensionless numbers represent the influence of the wetted area and the vapor flow resistance into the foam structure.

Once all the Π groups were identified, the new correlation for the pool boiling HTC on metal foams can be written as,

$$\frac{h \cdot L_c}{k_{\text{eff}}} = C_1 \left[\left(\frac{q'' \cdot L_c}{k_{\text{eff}} T_{\text{sat}}} \right)^{a_1} \left(\frac{c_{p,l} \mu_l}{k_{\text{eff}}} \right)^{a_2} \left(\frac{c_{p,l} T_{\text{sat}}}{h_{lv}} \right)^{a_3} \left(\frac{\delta}{L_c} \right)^{a_4} \left(\frac{d_p}{L_c} \right)^{a_5} \right] \quad (22)$$

where C_1 and the exponent a_i are constant, except a_4 , defined by the authors as a function of the heat flux,

$$a_4 = f(q'') = \frac{a}{b + \exp(c \cdot q'' - d)} - e \quad (23)$$

that is an inverse ‘S-shaped’ curve, which takes into account the effect of the thickness in the boiling curve of metal foams. At low heat fluxes, thicker foams result in higher HTC and vice-versa due to the balance of heat transfer area and vapor bubble flow resistance as reported by Manetti et al. [37].

The thermophysical properties of both working fluids used in the regression analysis are listed in **Table 5** (corresponds to the liquid saturated conditions on the average local atmospheric pressure where the tests were carried out).

Table 5. Thermophysical properties from HFE-7100 and ethanol at local atmospheric pressure.

Fluid	p_{atm} (kPa)	T_{sat} (°C)	ρ_l (kg/m ³)	ρ_v (kg/m ³)	$10^6 \times \mu_l$ (Pa.s)	$c_{p,l}$ (J/kg.K)	h_{lv} (kJ/kg)	k_l (W/m.K)	σ (mN/m)	L_c (mm)
HFE-7100	98*	60.3	1420.7	9.47	431	1253.6	111.9	0.062	10.26	0.86
Ethanol	100.6†	78.1	737.2	1.66	514	3111.0	849.4	0.157	17.62	1.56

*Atmospheric pressure at Ilha Solteira; †Atmospheric pressure at Lisbon

For the metal foams effective thermal conductivity, k_{eff} , it was used the model from Yao et al. [48],

$$k_{\text{eff}} = \left(\frac{\gamma}{k_A} + \frac{1 - 2\gamma}{k_B} + \frac{\gamma}{k_C} \right)^{-1} \quad (24)$$

where k_A , k_B e k_C are defined as:

$$k_A = \frac{5\sqrt{2}}{27} \pi \gamma (3 - 4\gamma) k_s + \left(1 - \frac{5\sqrt{2}}{27} \pi \gamma (3 - 4\gamma) \right) k_l \quad (25)$$

$$k_B = \frac{5\sqrt{2}}{27} \pi \gamma^2 k_s + \left(1 - \frac{10\sqrt{2}}{9} \pi \gamma^2 \right) k_l \quad (26)$$

$$k_C = \frac{5\sqrt{2}}{27} \pi \gamma^2 k_s + \left(1 - \frac{5\sqrt{2}}{27} \pi \gamma^2 \right) k_l \quad (27)$$

and γ is the ratio of the ligament node radii to the ligament length, which is a function of the porosity and can be obtained by,

$$\varepsilon = 1 - \frac{5\sqrt{2}}{8} \pi \gamma^2 (3 - 5\gamma) \quad (28)$$

The model from Yao et al. [48] was chosen due to the absence of an empirical factor for adjusting data with the experimental data from the same authors. Moreover, it was tested by Amani et al. [49] who also found a good agreement of the Yao et al. [48] model with the experimental and numerical simulation data.

Based on the regression analysis of the experimental database by using the least-squares method implemented on `SciPy`, a Python-based library, the following correlation was obtained with an R-square = 0.992:

$$\text{Nu} = \frac{h \cdot L_c}{k_{\text{eff}}} = 19.905 \left[\left(\frac{q'' L_c}{k_{\text{eff}} T_{\text{sat}}} \right)^{0.615} \left(\frac{c_{p,l} \mu_l}{k_{\text{eff}}} \right)^{0.322} \left(\frac{c_{p,l} T_{\text{sat}}}{h_{lv}} \right)^{-0.118} \left(\frac{\delta}{L_c} \right)^{f(q'')} \left(\frac{d_p}{L_c} \right)^{-0.200} \right] \quad (29)$$

where,

$$f(q'') = \frac{5.924}{25.327 + \exp(0.031 \times 10^{-3} q'' - 0.362)} - 0.037 \quad (30)$$

which returns a positive exponent for low heat fluxes and a negative exponent for high heat fluxes as shown in **Figure 11**.

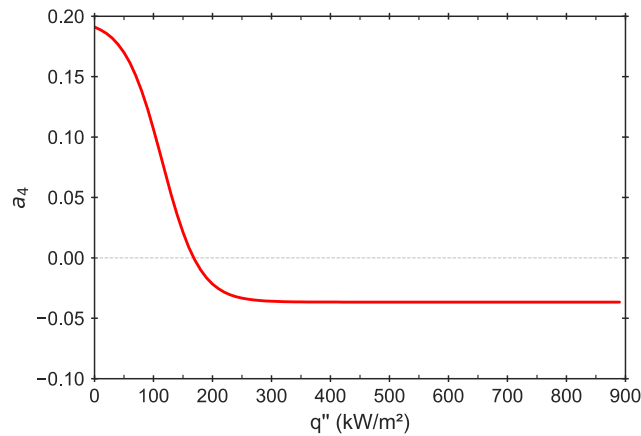


Figure 11. Exponent a_4 variation with the imposed heat flux.

Figure 12 shows the Nusselt number calculated by the Eq. (29), Nu_{calc} , *versus* the experimental Nusselt number, Nu_{exp} . The MAPE was 10.8% with 89.9% of the data fitted within the error range of $\pm 20\%$ and 93.8% within the error range of $\pm 30\%$. **Table 6** shows the statistical analysis of each surface used in the current work.

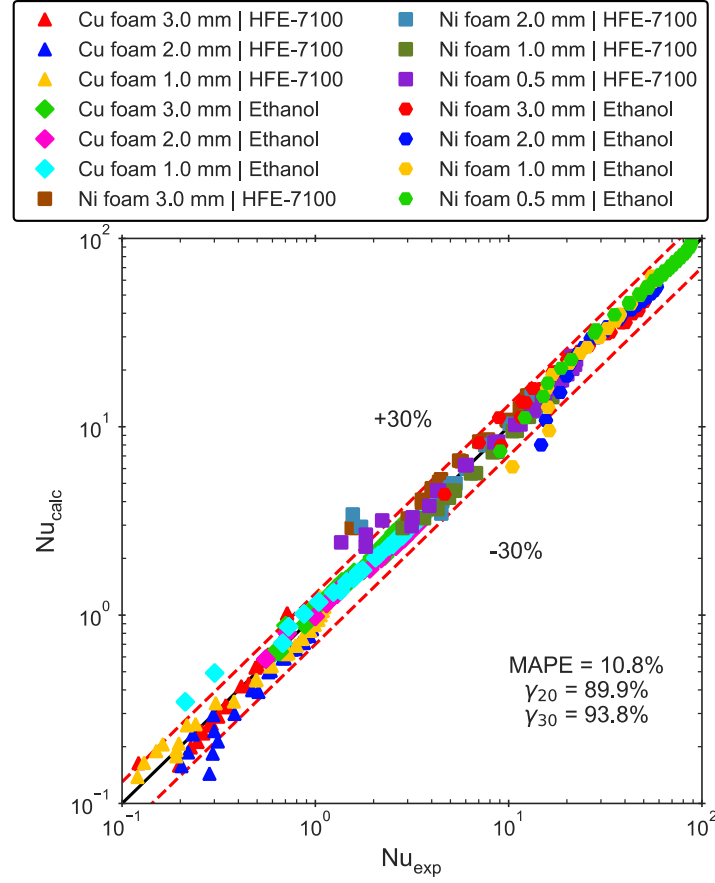


Figure 12. Comparison between predicted and experimental Nusselt number.

Table 6. Statistical analysis between experimental and predicted data for each surface used in the current study.

Surface	Fluid	MAPE	γ_{20}	γ_{30}
Cu foam 3.0 mm	HFE-7100	15.4%	72.7%	84.8%
Cu foam 2.0 mm	HFE-7100	15.4%	78.6%	89.3%
Cu foam 1.0 mm	HFE-7100	12.5%	86.1%	97.2%
Cu foam 3.0 mm	Ethanol	6.0%	96.3%	100.0%
Cu foam 2.0 mm	Ethanol	6.2%	100.0%	100.0%
Cu foam 1.0 mm	Ethanol	11.1%	90.5%	90.5%
Ni foam 3.0 mm	HFE-7100	16.7%	95.0%	95.0%
Ni foam 2.0 mm	HFE-7100	15.2%	85.0%	90.0%
Ni foam 1.0 mm	HFE-7100	10.6%	100.0%	100.0%
Ni foam 0.5 mm	HFE-7100	10.6%	87.9%	90.9%
Ni foam 3.0 mm	Ethanol	9.2%	96.6%	100.0%
Ni foam 2.0 mm	Ethanol	9.5%	88.9%	88.9%
Ni foam 1.0 mm	Ethanol	11.0%	80.6%	87.1%
Ni foam 0.5 mm	Ethanol	6.3%	100.0%	100.0%

4.1.1 HTC Predictive Model Validation

The validation step by using data from literature is to check if the proposed correlation is overfitted. So, the performance of the proposed correlation was evaluated by comparing it with 113 experimental data points obtained by other authors, namely by Atherya et al. [50], Moghaddam et al. [51], and Xu et al. [52]. Atherya et al. [50] used aluminum foams on boiling of FC-72 while Moghaddam et al. [51] used copper foams on boiling of FC-72; Xu et al. [52] used copper foams on boiling of acetone as the working fluid. Even though the working fluids are different from our experimental database, they were considered due to the wetting fluid behavior and dielectric characteristics. **Figure 13** shows the prediction of the independent experimental data from the literature. The MAPE was 19% with 58.6% of the data within an error range of $\pm 20\%$ and 79.5% within an error range of $\pm 30\%$. Besides, **Table 7** shows the individual error analysis.

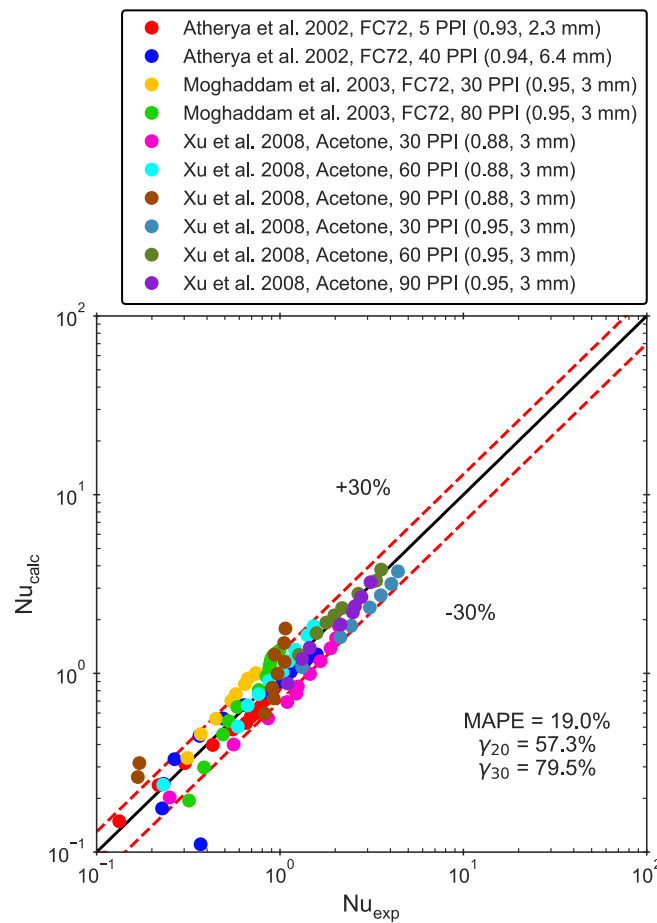


Figure 13. Comparison between the predicted Nusselt number and the experimental Nusselt number from the literature.

Table 7. Statistical analysis between predicted and experimental data from the literature.

Authors (year), fluid, metal foam characteristics	MAPE	γ_{20}	γ_{30}
Atherya et al. (2002), FC72, 5 PPI (0.93, 2.3 mm)	12.3%	100.0%	100.0%
Atherya et al. (2002), FC72, 40 PPI (0.94, 6.4 mm)	17.2%	75.0%	93.8%
Moghaddam et al. (2003), FC72, 30 PPI (0.95, 3 mm)	29.5%	11.1%	44.4%
Moghaddam et al. (2003), FC72, 80 PPI (0.95, 3 mm)	23.4%	35.7%	57.1%
Xu et al. (2008), Acetone, 30 PPI (0.88, 3 mm)	28.2%	18.2%	54.5%
Xu et al. (2008), Acetone, 60 PPI (0.88, 3 mm)	7.8%	90.0%	100.0%
Xu et al. (2008), Acetone, 90 PPI (0.88, 3 mm)	36.0%	27.3%	45.5%
Xu et al. (2008), Acetone, 30 PPI (0.95, 3 mm)	21.7%	28.6%	100.0%
Xu et al. (2008), Acetone, 60 PPI (0.95, 3 mm)	5.0%	100.0%	100.0%
Xu et al. (2008), Acetone, 90 PPI (0.95, 3 mm)	9.1%	87.5%	100.0%

We are aware that there are more works in the literature using metallic foams and dielectric fluids, however, only works that had the sufficient reported characteristics of the metallic foam (porosity, pore diameter, and thickness) could be checked by the new correlation.

4.2 Maximum Heat Flux Predictive Model Formulation

The model in Eq. (18) can predict the HTC but it does not have a limit to the imposed heat flux. As previously discussed, the metal foams can increase the boiling HTC; on the other hand, it can decrease or increase the dryout heat flux. So, there is a balance between the thickness and pore diameter due to the wetted area for heat transfer and vapor flow resistance. Therefore, to determine the maximum heat flux, q''_{\max} , corresponding to the heat flux value in which the HTC turning point occurs, we developed a second correlation that was based on the Buckingham π theorem [43]. The following parameters play role in the q''_{\max} for wetting dielectric fluids on metal foams:

- the first parameter is the reference heat flux, $q''_0 = \rho_v^{0.5} h_{lv} [\sigma g (\rho_l - \rho_v)]^{1/4}$, which is presented in most of the models which try to predict the CHF, as reported by Liang and Mudawar [53,54];
- the following two parameters represent the metal foam characteristics: the thickness (δ) and the pore diameter (d_p);
- the last two parameters are related to the working fluid: saturated liquid density (ρ_l) and saturated vapor density (ρ_v).

Thus, the following functional relation can be written:

$$q''_{\max} = f(q''_0, \delta, d_p, \rho_l, \rho_v) \quad (31)$$

The $n = 6$ variables are listed in the dimension MLT [44] that implies in $r = j = 3$ repeating variables (q''_0, d_p, ρ_l) resulting in $k = n - j = 3$ dimensionless variables (Π_k) .

The first dimensionless number obtained is,

$$\Pi_1 = \frac{q''_{\max}}{q''_0} \quad (32)$$

which captures the established dependence of maximum heat flux on the fluid properties and gravity [55].

The second dimensionless number is the metal foam length ratio,

$$\Pi_2 = \frac{\delta}{d_p} \quad (33)$$

which means the balance between the foam thickness and pore diameter/area density.

The third dimensionless number is the working fluid density ratio,

$$\Pi_3 = \frac{\rho_v}{\rho_l} \quad (34)$$

which is associated with the fluid expansion due to the phase-change.

Once all the Π groups were identified, the model which predict the maximum heat flux to pool boiling on metal foams can be written as,

$$\frac{q''_{\max}}{q''_0} = C_2 \left[\left(\frac{\delta}{d_p} \right)^{b_1} \left(\frac{\rho_v}{\rho_l} \right)^{b_2} \right] \quad (35)$$

where C_2 and the exponent b_i are constants.

The experimental maximum heat flux, $q''_{\max, \text{exp}}$, is given by the heat flux in which the experimental HTC is maximum. Such values are strongly dependent on the applied heat flux and these maximum values may not match the true value. So, instead of using $q''_{\max, \text{exp}}$, it was

carried out a polynomial regression on each experimental HTC curve and the maximum heat flux was obtained by the polynomial curve turning point, $q''_{\max,\text{pol}}$ (**Figure 14**).

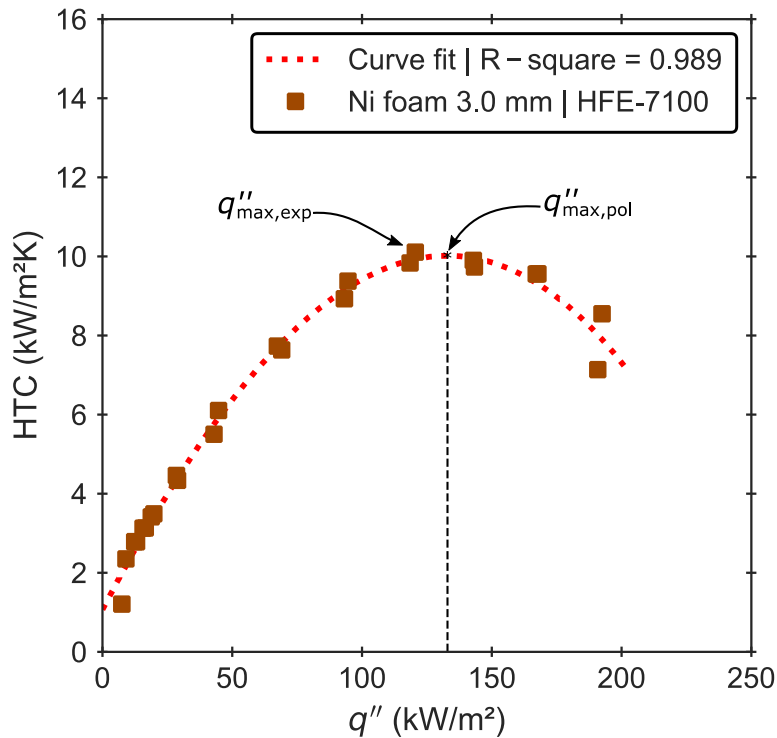


Figure 14. Comparison of the maximum heat flux for the HTC experimental curve and the third-degree polynomial curve fit.

In this way, we tested second and third-degree polynomials regression and realize that the regression by using third-degree polynomial, $y = ax^3 + bx^2 + cx + d$, obtained an R-square coefficient greater than the second degree in all cases. Besides, the third-degree polynomial regression curves presented more consistency with the experimental boiling HTC curve. **Table 8** shows the maximum heat flux from the experimental HTC curve and the polynomial curve fit turning point, as well as, its R-square.

Table 8. Maximum heat flux, experimental and polynomial, for all conditions tested in the current study.

Surface	Fluid	$q''_{\max,\text{exp}}$ (kW/m ²)	$q''_{\max,\text{pol}}$ (kW/m ²)	R-square
Cu foam 3.0 mm	HFE-7100	223.38	231.34	0.991
Cu foam 2.0 mm	HFE-7100	264.95	267.49	0.991
Cu foam 1.0 mm	HFE-7100	344.97	330.83	0.998
Cu foam 3.0 mm	Ethanol	321.37	372.84	0.982
Cu foam 2.0 mm	Ethanol	485.81	471.20	0.998
Cu foam 1.0 mm	Ethanol	663.11	638.70	0.994
Ni foam 3.0 mm	HFE-7100	120.55	132.94	0.989
Ni foam 2.0 mm	HFE-7100	118.31	127.12	0.968
Ni foam 1.0 mm	HFE-7100	171.47	183.26	0.994
Ni foam 0.5 mm	HFE-7100	302.03	295.95	0.997
Ni foam 3.0 mm	Ethanol	308.25	325.60	0.998
Ni foam 2.0 mm	Ethanol	368.72	403.27	0.998
Ni foam 1.0 mm	Ethanol	439.38	401.46	0.989
Ni foam 0.5 mm	Ethanol	842.16	883.29	0.999

Based on the regression analysis of the experimental database by using the least-squares method implemented on `SciPy`, the following correlation was obtained with an R-square = 0.820:

$$\frac{q''_{\max}}{q''_0} = 1.684 \left[\left(\frac{\delta}{d_p} \right)^{-0.487} \left(\frac{\rho_v}{\rho_l} \right)^{0.300} \right] \quad (36)$$

Figure 15 shows the heat flux ratio calculated by the Eq. (36) *versus* the polynomial, $q''_{\max,\text{pol}}/q''_0$, obtained based on the current work experimental data. The MAPE was 13.6% with 71.4% of the data fitted within the error range of $\pm 20\%$ and 100% within the error range of $\pm 30\%$. **Table 9** shows the absolute percentage error (APE) of each surface used in the current work.

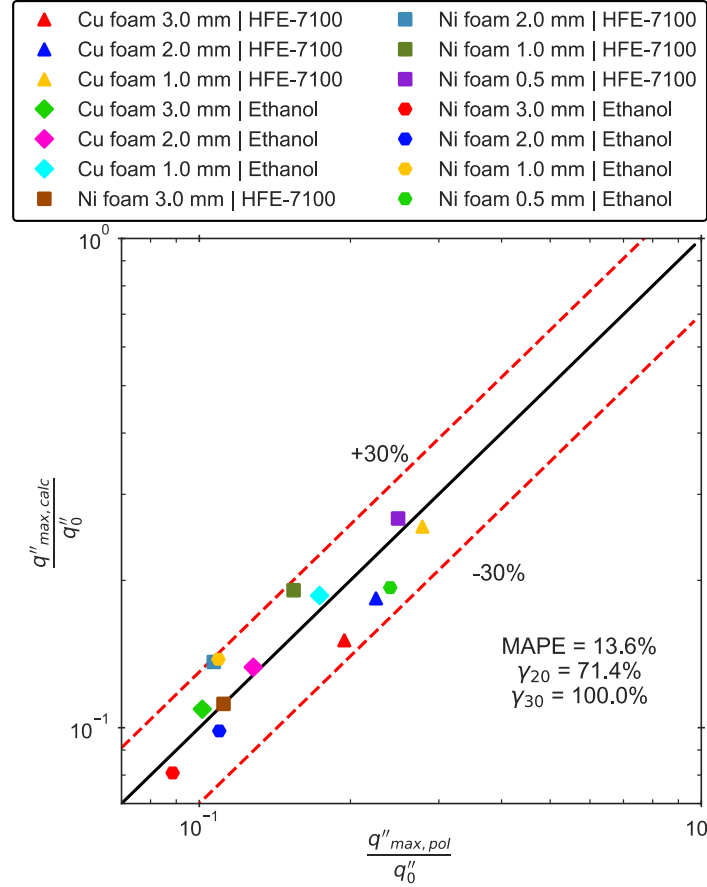


Figure 15. Maximum heat flux heat comparison between experimental data and the predicted data by the proposed model.

Table 9. Absolute percentage error between the maximum heat flux calculated by Eq. (35) and the polynomial obtained by fitting the experimental curve.

Surface	Fluid	APE*
Cu foam 3.0 mm	HFE-7100	22.4%
Cu foam 2.0 mm	HFE-7100	18.2%
Cu foam 1.0 mm	HFE-7100	7.4%
Cu foam 3.0 mm	Ethanol	7.6%
Cu foam 2.0 mm	Ethanol	3.8%
Cu foam 1.0 mm	Ethanol	7.2%
Ni foam 3.0 mm	HFE-7100	0.1%
Ni foam 2.0 mm	HFE-7100	27.5%
Ni foam 1.0 mm	HFE-7100	23.9%
Ni foam 0.5 mm	HFE-7100	7.5%
Ni foam 3.0 mm	Ethanol	8.7%
Ni foam 2.0 mm	Ethanol	10.2%
Ni foam 1.0 mm	Ethanol	26.4%
Ni foam 0.5 mm	Ethanol	19.5%

$$* \text{APE} = \frac{|q''_{\max, \text{calc}} - q''_{\max, \text{pol}}|}{q''_{\max, \text{pol}}}$$

4.2.1 Maximum Heat Flux Predictive Model Validation

Data from the literature were used to validate the maximum heat flux model. The experimental HTC curves from the literature were fitted by the third-degree polynomial curve with an R-square > 0.9. **Figure 16** shows the heat flux ratio calculated by the Eq. (35) *versus* the polynomial, $q''_{\max, \text{pol}}/q''_0$, obtained from the literature experimental data. The MAPE was 52.2% with 40.0% of the data fitted within the error range of $\pm 20\%$ and 50.0% within the error range of $\pm 30\%$. **Table 10** shows the absolute percentage error (APE) of each surface used in the current work.

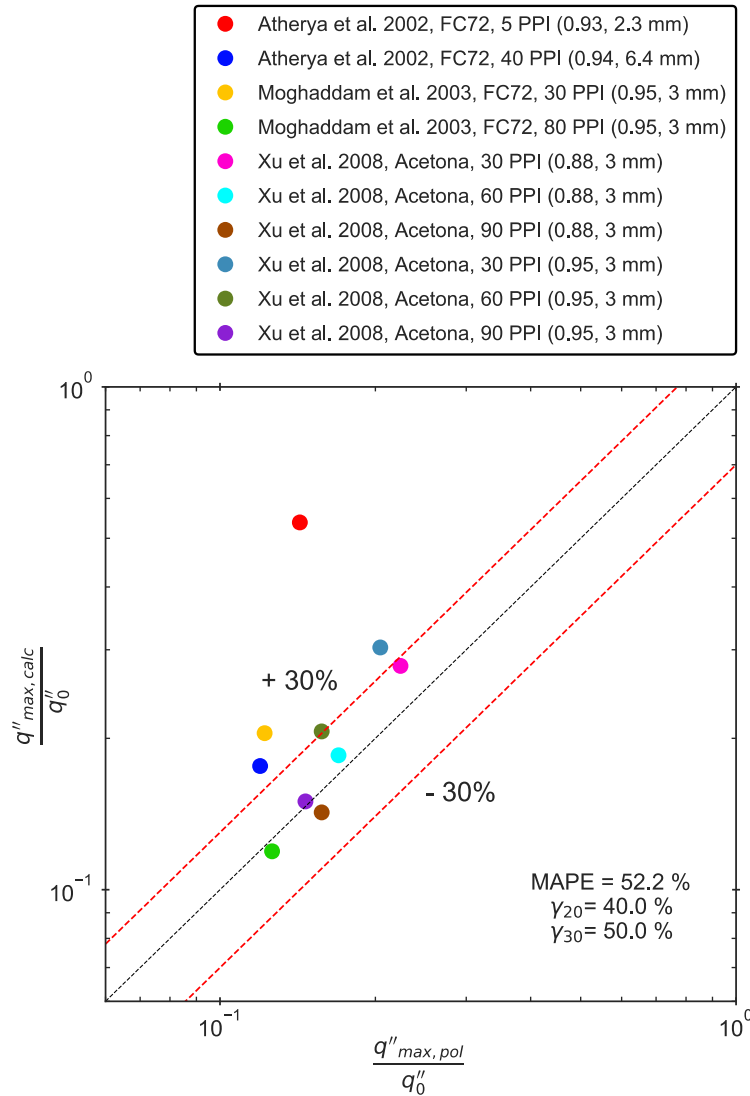


Figure 16. Maximum heat flux heat comparison between the predicted data by the proposed model and data from the literature.

Table 10. Absolute percentage error between the maximum heat flux calculated by Eq. (35) and the polynomial fitting curve.

Authors (year), fluid, metal foam characteristics	APE
Atherya et al. (2002), FC72, 5 PPI (0.93, 2.3 mm)	276.4%
Atherya et al. (2002), FC72, 40 PPI (0.94, 6.4 mm)	47.3%
Moghaddam et al. (2003), FC72, 30 PPI (0.95, 3 mm)	67.8%
Moghaddam et al. (2003), FC72, 80 PPI (0.95, 3 mm)	5.5%
Xu et al. (2008), Acetone, 30 PPI (0.88, 3 mm)	24.5%
Xu et al. (2008), Acetone, 60 PPI (0.88, 3 mm)	9.1%
Xu et al. (2008), Acetone, 90 PPI (0.88, 3 mm)	9.5%
Xu et al. (2008), Acetone, 30 PPI (0.95, 3 mm)	48.3%
Xu et al. (2008), Acetone, 60 PPI (0.95, 3 mm)	31.2%
Xu et al. (2008), Acetone, 90 PPI (0.95, 3 mm)	2.3%

The APE, for Atherya et al. [50] case, was higher than the HTC model validation because 5 PPI metal foam (the red outline point in **Figure 16**) had a pore diameter higher than the pore diameters used to fit the model. However, for the HTC predictive model, data from Atherya et al. [50] with 5 PPI showed a good coherency probably due to the HTC model be lesser sensible to the pore diameter than the maximum heat flux model.

4.3 Pore diameter determination from PPI and porosity

To develop the previous models we used the pore diameter as one of the main dimensions of the metal foam. The dimension was obtained from image analysis as presented in Section 2. However, the commercial metal foams are usually found in terms of PPI and porosity (or relative density); thus, the pore diameter value can be hard to find and, consequently, the model application is unsolved. So, a solution is to use the geometric model available in the literature, which is a function of both PPI and porosity, to solve the pore diameter and fiber diameter. The Calmidi [56] model improved by Bhattacharya et al. [57] yields,

$$\text{PPI} = \frac{1}{d_p + d_f} \quad (37)$$

and,

$$\frac{d_f}{d_p} = 3.39 \sqrt{\frac{1 - \varepsilon}{3\pi}} \cdot \frac{1}{G} \quad (38)$$

where,

$$G = 1 - \exp\left(-\frac{1 - \varepsilon}{0.04}\right) \quad (39)$$

These equations can be easily solved since the PPI and porosity are known. We calculated the pore diameter by using Eq. (37) and Eq. (38) using as input the PPI and porosity presented in Section 2; the predicted pore diameters were 0.58 mm and 0.29 mm for Cu foam and Ni foam, respectively.

To check the validity of predicted pore diameters, the experimental database was tested in the HTC predictive model, Eq. (29), and in the maximum heat flux model, Eq.(36), by using the predicted pore diameters instead of those presented in **Table 2**. The HTC predictive model presented a MAPE equal to 10.8%, *i.e.*, the same as **Figure 12**. The maximum heat flux model presented a MAPE equal to 16.3%, which is just 2.7% higher than that in **Figure 15**. Therefore, the Bhattacharya et al. [57] prediction model for the metal foam pore diameter can be applied in our models in those cases that the d_p is unknown.

4.4 Model Sensibility

To check the behavior of both new models obtained in the current work we coupled them; so, the Eq. (29) is valid between the range of heat flux from 0 to q''_{\max} given by Eq. (36). **Figure 17** shows the sensibility of coupled models for each characteristic of metal foam: (a) pore diameter, (b) thickness, (c) porosity, and (d) metal foam solid-phase thermal conductivity. Moreover, the last figure (f) shows the sensibility with different working fluids.

The pore diameter plays a role in both models since, as it increases, the heat flux range increases and the HTC decreases. The thickness has an opposite behavior in the heat flux range, *i.e.*, as it increases the heat flux range decreases; for the HTC it is quite similar however, it is possible to note the influence of Eq. (30): as the thickness increases for low heat fluxes, the HTC increases up to 175 kW/m² and, after that, thinner foams have a better performance.

Another variable that plays a role in the model is the porosity, which does not appear explicitly in Eq. (29) but it is included in the effective thermal conductivity given by Eq. (24) to Eq. (28). Lower porosities have better HTC performance since they have higher effective thermal conductivity, which is a variable in the Nusselt number. In the same way, increasing the solid thermal conductivity, k_s - the thermal conductivity from the solid phase of the metal

foam - the HTC also increases; the values used in **Figure 17** (d) are from stainless steel, nickel, aluminum, and copper, respectively, which are the most used materials for metal foams. Finally, different wetting and dielectric working fluid are shown in **Figure 17**; among the four fluids selected, ethanol was the one that showed better performance mainly due to the latent heat of vaporization, liquid thermal conductivity, and saturation temperature.

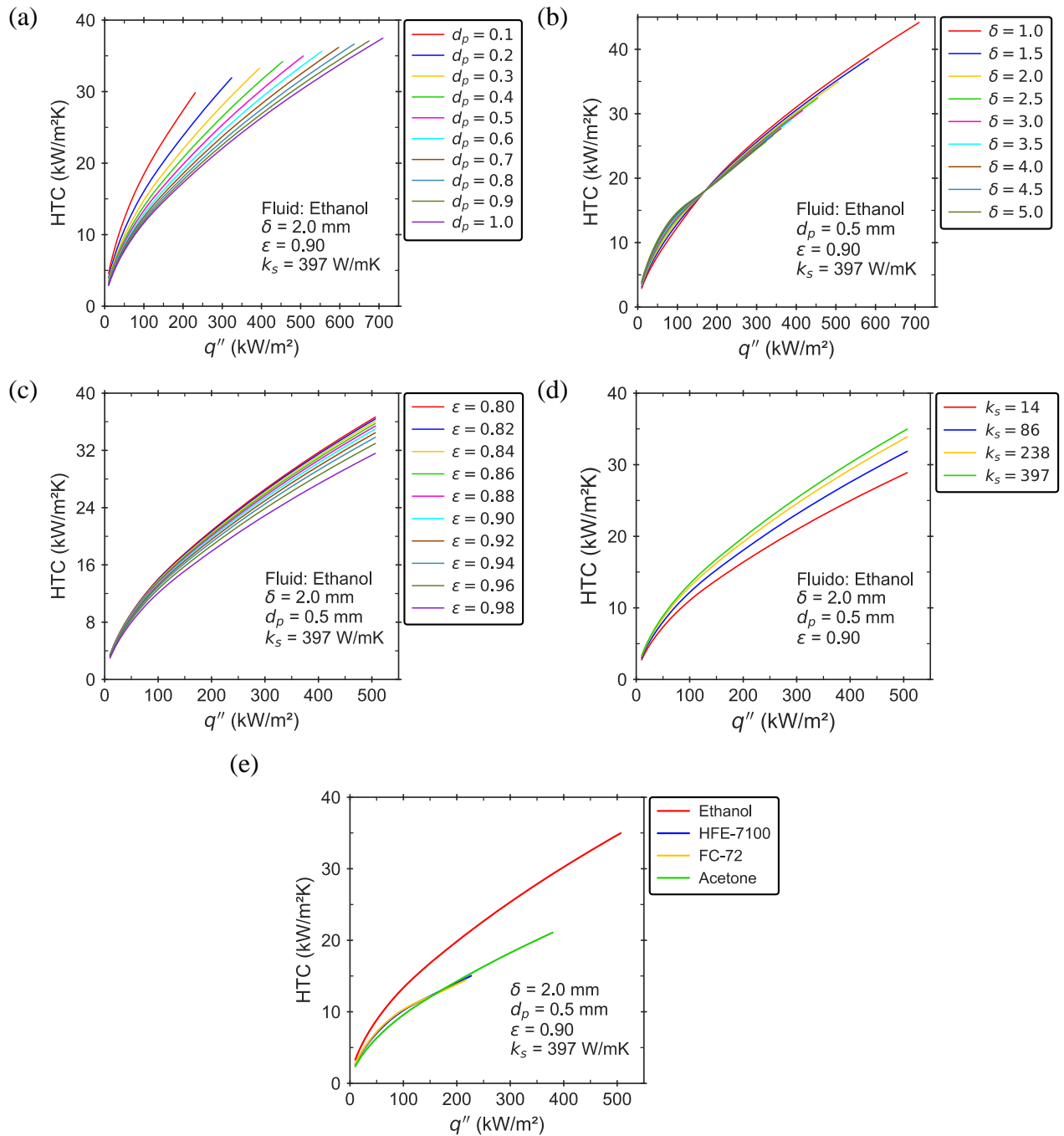


Figure 17. Coupled models sensibility: (a) pore diameter variation [mm]; (b) thickness variation [mm]; (c) porosity variation; (d) solid material thermal conductivity variation [W/m.K]; and, (f) working fluids variation.

5. Final Remarks

In this work we developed a semi-empirical correlation, based on dimensional analysis, for metal foams surfaces in pool boiling with a dielectric fluid, taking into account the porous heating surface characteristics (porosity, pore diameter, and thickness), the working fluid thermophysical properties, and the interaction between them. The correlation was developed based on our experimental database and validated with the open literature database. The following conclusion can be drawn:

- For the newly HTC predictive model, Eq. (29), the MAPE is 10.8% with 89.9% of the data fitted within the error range of $\pm 20\%$ and 93.8% within the error range of $\pm 30\%$. By comparing it with experimental data points obtained by other authors from the literature, the MAPE is 19% with 79.5% within an error range of $\pm 30\%$.
- To complement the HTC predictive model, we also develop a model to predict the maximum heat flux (q''_{\max}), Eq. (36), corresponding to the heat flux value in which the HTC turning point occurs. To the maximum heat flux model, for the comparison with the experimental database, the MAPE is 13.6% with 100% within the error range of $\pm 30\%$.
- The Bhattacharya et al. [57] prediction model for the metal foam pore diameter can be applied in our models - HTC predictive model, Eq. (29), and in the maximum heat flux model, Eq. (36) - in those cases that the d_p is unknown.
- The thickness level variation plays an important role in the boiling curves as well as pore diameter. Both can result in a better heat transfer performance when well combined. At low heat fluxes values, thicker foams can increase the HTC due to the wetted area; however, at high heat fluxes, it decreases the HTC due to the vapor bubble flow resistance and vice-versa. For the pore diameter, it is observed the opposite effect: smaller pores increase the HTC at low heat fluxes values and decrease it at high heat fluxes. So, the thicker and smaller the pores, the larger the liquid-vapor counter-flow since the liquid replenishment is inhibited, leading to a lower HTC and an earlier occurrence of dryout.
- The metal foam porosity and solid-phase thermal conductivity also play an important role in the HTC model. The lower the porosities the higher the HTC, due to the higher effective thermal conductivity. In the same way, as the solid-phase thermal conductivity increases the HTC also increases.

- The model is sensitive to the metal foams characteristics however, the influence of the working fluid thermophysical properties on the HTC predictive model is more pronounced.

Acknowledgments

The authors are grateful for the financial support from the PPGEM – UNESP/FEIS, from CAPES, from the National Council of Technological and Scientific Development of Brazil (CNPq grant number 458702/2014-5) and FAPESP (grant number 2013/15431-7; 2017/13813-0; 2019/02566-8, 2019/15250-9). The authors also acknowledge FCT for partially financing the work through project JICAM/0003/2017.

References

- [1] S. Fan, F. Duan, A review of two-phase submerged boiling in thermal management of electronic cooling, *International Journal of Heat and Mass Transfer*. 150 (2020) 119324. <https://doi.org/10.1016/j.ijheatmasstransfer.2020.119324>.
- [2] L. Duan, B. Liu, B. Qi, Y. Zhang, J. Wei, Pool boiling heat transfer on silicon chips with non-uniform micro-pillars, *International Journal of Heat and Mass Transfer*. 151 (2020) 119456. <https://doi.org/10.1016/j.ijheatmasstransfer.2020.119456>.
- [3] A. Mehralizadeh, S. Reza Shabanian, G. Bakeri, Effect of modified surfaces on bubble dynamics and pool boiling heat transfer enhancement: A review, *Thermal Science and Engineering Progress*. 15 (2020) 100451. <https://doi.org/10.1016/j.tsep.2019.100451>.
- [4] P. Tuma, Evaporator/boiler design for thermosyphons utilizing segregated hydrofluoroether working fluids, in: *Twenty-Second Annual IEEE Semiconductor Thermal Measurement And Management Symposium*, IEEE, 2006: pp. 69–77. <https://doi.org/10.1109/STHERM.2006.1625209>.
- [5] M.S. El-Genk, Nucleate boiling enhancements on porous graphite and microporous and macro-finned copper surfaces, *Heat Transfer Engineering*. 33 (2012) 175–204. <https://doi.org/10.1080/01457632.2011.589305>.
- [6] V. Abreu, M. Harrison, J. Gess, A.S. Moita, Two-Phase Thermosiphon Cooling Using Integrated Heat Spreaders With Copper Microstructures, in: *2018 17th IEEE Intersociety Conference on Thermal and Thermomechanical Phenomena in Electronic Systems (ITherm)*, IEEE, 2018: pp. 645–652. <https://doi.org/10.1109/ITHERM.2018.8419644>.
- [7] K.K. Wong, K.C. Leong, Saturated pool boiling enhancement using porous lattice structures produced by Selective Laser Melting, *International Journal of Heat and Mass Transfer*. 121 (2018) 46–63. <https://doi.org/10.1016/j.ijheatmasstransfer.2017.12.148>.
- [8] G. Liang, I. Mudawar, Review of pool boiling enhancement by surface modification, *International Journal of Heat and Mass Transfer*. 128 (2019) 892–933. <https://doi.org/10.1016/j.ijheatmasstransfer.2018.09.026>.

- [9] T.J. Hendricks, S. Krishnan, C. Choi, C. Chang, B. Paul, Enhancement of pool-boiling heat transfer using nanostructured surfaces on aluminum and copper, *International Journal of Heat and Mass Transfer*. 53 (2010) 3357–3365. <https://doi.org/10.1016/j.ijheatmasstransfer.2010.02.025>.
- [10] M. Shojaeian, A. Koşar, Pool boiling and flow boiling on micro- and nanostructured surfaces, *Experimental Thermal and Fluid Science*. 63 (2015) 45–73. <https://doi.org/10.1016/j.expthermflusci.2014.12.016>.
- [11] L. Lin, M.A. Kedzierski, Review of low-GWP refrigerant pool boiling heat transfer on enhanced surfaces, *International Journal of Heat and Mass Transfer*. 131 (2019) 1279–1303. <https://doi.org/10.1016/j.ijheatmasstransfer.2018.11.142>.
- [12] Z. Wu, Z. Cao, B. Sundén, Saturated pool boiling heat transfer of acetone and HFE-7200 on modified surfaces by electrophoretic and electrochemical deposition, *Applied Energy*. 249 (2019) 286–299. <https://doi.org/10.1016/j.apenergy.2019.04.160>.
- [13] R.W. Bowring, Physical model, based on bubble detachment, and calculation of steam voidage in the sub-cooled region of a heated channel, Institutt for Atomenergi (Norway). OECD Halden Reaktor Prosjekt, 1962.
- [14] C. Gerardi, J. Buongiorno, L. wen Hu, T. McKrell, Study of bubble growth in water pool boiling through synchronized, infrared thermometry and high-speed video, *International Journal of Heat and Mass Transfer*. 53 (2010) 4185–4192. <https://doi.org/10.1016/j.ijheatmasstransfer.2010.05.041>.
- [15] S.J. Thiagarajan, R. Yang, C. King, S. Narumanchi, Bubble dynamics and nucleate pool boiling heat transfer on microporous copper surfaces, *International Journal of Heat and Mass Transfer*. 89 (2015) 1297–1315. <https://doi.org/10.1016/j.ijheatmasstransfer.2015.06.013>.
- [16] Z. Cao, Z. Wu, B. Sundén, Heat transfer prediction and critical heat flux mechanism for pool boiling of NOVEC-649 on microporous copper surfaces, *International Journal of Heat and Mass Transfer*. 141 (2019) 818–834. <https://doi.org/10.1016/j.ijheatmasstransfer.2019.07.036>.
- [17] W.M. Rohsenow, A method of correlating heat transfer data for surface boiling of liquids, *Transactions of ASME – Journal of Heat Transfer*. 74 (1952) 969–976.
- [18] K. Stephan, M. Abdelsalam, Heat-transfer correlations for natural convection boiling, *International Journal of Heat and Mass Transfer*. 23 (1980) 73–87. [https://doi.org/10.1016/0017-9310\(80\)90140-4](https://doi.org/10.1016/0017-9310(80)90140-4).
- [19] E. Teodori, A.S. Moita, A.L.N. Moreira, Empirical and Modeling-Based Correlations for Pool Boiling on Microstructured Surfaces, *Interfacial Phenomena and Heat Transfer*. 2 (2014) 273–292. <https://doi.org/10.1615/interfacphenomheattransfer.2015011663>.
- [20] I.S. Kiyomura, T.S. Mogaji, L.L. Manetti, E.M. Cardoso, A predictive model for confined and unconfined nucleate boiling heat transfer coefficient, *Applied Thermal Engineering*. 127 (2017) 1274–1284. <https://doi.org/10.1016/j.applthermaleng.2017.08.135>.
- [21] J.M. Jabardo, E. Silva, G. Ribatski, S.F. de Barros, Evaluation of the Rohsenow correlation through experimental pool boiling of halocarbon refrigerants on cylindrical surfaces, *Journal of the Brazilian Society of Mechanical Sciences and Engineering*. 26 (2004) 218–230.

- [22] K. Stephan, *Heat Transfer in Condensation and Boiling*, Springer Berlin Heidelberg, Berlin, Heidelberg, 1992. <https://doi.org/10.1007/978-3-642-52457-8>.
- [23] G. Liang, Y. Chen, H. Yang, D. Li, S. Shen, Nucleate boiling heat transfer and critical heat flux (CHF) from micro-pit surfaces, *International Journal of Heat and Mass Transfer*. 152 (2020) 119510. <https://doi.org/10.1016/j.ijheatmasstransfer.2020.119510>.
- [24] K. Nishikawa, T. Ito, Augmentation of nucleate boiling heat transfer by prepared surfaces, *Heat Transfer in Energy Problems*. (1982) 111–118.
- [25] Z.G. Xu, Z.G. Qu, C.Y. Zhao, W.Q. Tao, Experimental correlation for pool boiling heat transfer on metallic foam surface and bubble cluster growth behavior on grooved array foam surface, *International Journal of Heat and Mass Transfer*. 77 (2014) 1169–1182. <https://doi.org/10.1016/j.ijheatmasstransfer.2014.06.037>.
- [26] G. Righetti, L. Doretto, H. Sadafi, K. Hooman, Water pool boiling across low pore density aluminum foams, *Heat Transfer Engineering*. 0 (2019) 1–10. <https://doi.org/10.1080/01457632.2019.1640464>.
- [27] H. Hu, Y. Zhao, Z. Lai, C. Hu, Experimental investigation on nucleate pool boiling heat transfer characteristics on hydrophobic metal foam covers, *Applied Thermal Engineering*. 179 (2020) 115730. <https://doi.org/10.1016/j.applthermaleng.2020.115730>.
- [28] J. Shi, X. Jia, D. Feng, Z. Chen, C. Dang, Wettability effect on pool boiling heat transfer using a multiscale copper foam surface, *International Journal of Heat and Mass Transfer*. 146 (2020) 118726. <https://doi.org/10.1016/j.ijheatmasstransfer.2019.118726>.
- [29] Z.-G. Xu, Z.-G. Qu, D.-G. Li, C.-Y. Zhao, W.-Q. Tao, T.-J. Lu, M.-Q. Wang, Experimental study of pool boiling on surface of metal foam with open cells, *Kung Cheng Je Wu Li Hsueh Pao/Journal of Engineering Thermophysics*. 30 (2009) 1713–1716.
- [30] K.P. Burnham, D.R. Anderson, *Model Selection and Multimodel Inference: A Practical Information-Theoretic Approach*, 2nd ed., Springer-Verlag, New York, 2002. <https://doi.org/10.1007/b97636>.
- [31] M.F. Ashby, T. Evans, N.A. Fleck, J.W. Hutchinson, H.N.G. Wadley, L.J. Gibson, *Metal foams: a design guide*, Elsevier, 2000.
- [32] J. Banhart, Manufacture, characterization and application of cellular metals and metal foams, *Progress in Materials Science*. 46 (2001) 559–632.
- [33] E. Brun, J. Vicente, F. Topin, R. Occelli, IMorph: A 3D morphological tool to fully analyze all kind of cellular materials, *Cellular Metals for Structural and Functional Applications*. (2008).
- [34] J. Vicente, F. Topin, J.-V. Daurelle, Open Celled Material Structural Properties Measurement: From Morphology To Transport Properties, *Mater. Trans.* 47 (2006) 2195–2202. <https://doi.org/10.2320/matertrans.47.2195>.
- [35] J. Mollicone, F. Ansart, P. Lenormand, B. Duployer, C. Tenailleau, J. Vicente, Characterization and functionalization by sol-gel route of SiC foams, *Journal of the European Ceramic Society*. 34 (2014) 3479–3487. <https://doi.org/10.1016/j.jeurceramsoc.2014.05.030>.
- [36] Online Materials Information Resource - MatWeb, (n.d.). <http://www.matweb.com/> (accessed September 1, 2020).

- [37] L.L. Manetti, A.S.O.H. Moita, R.R. de Souza, E.M. Cardoso, Effect of copper foam thickness on pool boiling heat transfer of HFE-7100, *International Journal of Heat and Mass Transfer*. 152 (2020) 119547. <https://doi.org/10.1016/j.ijheatmasstransfer.2020.119547>.
- [38] L.L. Manetti, G. Ribatski, R.R. de Souza, E.M. Cardoso, Pool boiling heat transfer of HFE-7100 on metal foams, *Experimental Thermal and Fluid Science*. 113 (2020) 110025. <https://doi.org/10.1016/j.expthermflusci.2019.110025>.
- [39] P. Pontes, R. Cautela, E. Teodori, A. Moita, Y. Liu, A.L.N. Moreira, A. Nikulin, E.P. del Barrio, Effect of pattern geometry on bubble dynamics and heat transfer on biphilic surfaces, *Experimental Thermal and Fluid Science*. 115 (2020) 110088. <https://doi.org/10.1016/j.expthermflusci.2020.110088>.
- [40] P. Pontes, R. Cautela, E. Teodori, A.S. Moita, A. Georgoulas, A.L.N.M. Moreira, Bubble Dynamics and Heat Transfer on Biphilic Surfaces: Experiments and Numerical Simulation, *J Bionic Eng*. 17 (2020) 809–821. <https://doi.org/10.1007/s42235-020-0064-x>.
- [41] R.J. Moffat, Describing the uncertainties in experimental results, *Experimental Thermal and Fluid Science*. 1 (1988) 3–17.
- [42] V.V. Calmidi, R.L. Mahajan, Forced convection in high porosity metal foams, *Journal of Heat Transfer*. 122 (2000) 557–565. <https://doi.org/10.1115/1.1287793>.
- [43] E. Buckingham, On physically similar systems; illustrations of the use of dimensional equations, *Physical Review*. 4 (1914) 345.
- [44] F.M. White, *Fluid mechanics*, 6th ed, McGraw-Hill, New York, NY, 2009.
- [45] C.W. Somerton, The Prandtl number effect in porous layer convection, *Applied Scientific Research*. 40 (1983) 333–344.
- [46] V. Kathare, J.H. Davidson, F.A. Kulacki, Natural convection in water-saturated metal foam, *International Journal of Heat and Mass Transfer*. 51 (2008) 3794–3802. <https://doi.org/10.1016/j.ijheatmasstransfer.2007.11.051>.
- [47] N. Dukhan, K.-C. Chen, Heat transfer measurements in metal foam subjected to constant heat flux, *Experimental Thermal and Fluid Science*. 32 (2007) 624–631. <https://doi.org/10.1016/j.expthermflusci.2007.08.004>.
- [48] Y. Yao, H. Wu, Z. Liu, A new prediction model for the effective thermal conductivity of high porosity open-cell metal foams, *International Journal of Thermal Sciences*. 97 (2015) 56–67.
- [49] Y. Amani, A. Takahashi, P. Chantrenne, S. Maruyama, S. Dancette, E. Maire, Thermal conductivity of highly porous metal foams: Experimental and image-based finite element analysis, *International Journal of Heat and Mass Transfer*. 122 (2018) 1–10.
- [50] B.P. Athreya, R.L. Mahajan, S. Sett, Pool boiling of FC-72 over metal foams: Effect of foam orientation and geometry, 8th AIAA/ASME Joint Thermophysics and Heat Transfer Conference. (2002) 1–10.
- [51] S. Moghaddam, M. Ohadi, J. Qi, Pool Boiling of Water and FC-72 on Copper and Graphite Foams, in: 2003 International Electronic Packaging Technical Conference and Exhibition, Volume 2, ASME, 2003: pp. 675–680. <https://doi.org/10.1115/IPACK2003-35316>.

- [52] J. Xu, X. Ji, W. Zhang, G. Liu, Pool boiling heat transfer of ultra-light copper foam with open cells, *International Journal of Multiphase Flow*. 34 (2008) 1008–1022. <https://doi.org/10.1016/j.ijmultiphaseflow.2008.05.003>.
- [53] G. Liang, I. Mudawar, Pool boiling critical heat flux (CHF) – Part 1: Review of mechanisms, models, and correlations, *International Journal of Heat and Mass Transfer*. 117 (2018a) 1352–1367. <https://doi.org/10.1016/j.ijheatmasstransfer.2017.09.134>.
- [54] G. Liang, I. Mudawar, Pool boiling critical heat flux (CHF) – Part 2: Assessment of models and correlations, *International Journal of Heat and Mass Transfer*. 117 (2018b) 1368–1383. <https://doi.org/10.1016/j.ijheatmasstransfer.2017.09.073>.
- [55] H. O’Hanley, C. Coyle, J. Buongiorno, T. McKrell, L.-W. Hu, M. Rubner, R. Cohen, Separate effects of surface roughness, wettability, and porosity on the boiling critical heat flux, *Appl. Phys. Lett.* 103 (2013) 024102. <https://doi.org/10.1063/1.4813450>.
- [56] V.V. Calmidi, Transport phenomena in high porosity fibrous metal foams., Ph.D. Thesis, University of Colorado, 1998.
- [57] A. Bhattacharya, R.L. Mahajan, Finned metal foam heat sinks for electronics cooling in forced convection, *Journal of Electronic Packaging, Transactions of the ASME*. 124 (2002) 155–163. <https://doi.org/10.1115/1.1464877>.

Declaration of Competing Interest

The authors declare that they have no known competing financial interests or personal relationships that could have appeared to influence the work reported in this paper.

Author Statement

L.L. Manetti: Methodology, Validation, Investigation, Data curation, Formal analysis, Writing - Original Draft, Writing - Review & Editing

E.M. Cardoso: Conceptualization, Funding acquisition, Project administration, Supervision, Methodology, Formal analysis, Writing - Original Draft, Writing - Review & Editing

A.S. Moita: Conceptualization, Supervision, Project administration, Methodology, Formal analysis, Resources, Writing - Original Draft, Writing - Review & Editing